INVESTIGATING SOLUBLE ORGANIC COMPOUNDS IN AQUEOUSLY ALTERED CARBONACEOUS CHONDRITES BY ULTRAHIGH RESOLUTION ORBITRAP MASS SPECTROMETRY

by

Patrick Kyle Schwartz

A thesis

submitted in partial fulfillment

of the requirements for the degree of

Master of Science in Chemistry

Boise State University

August 2019

BOISE STATE UNIVERSITY GRADUATE COLLEGE

DEFENSE COMMITTEE AND FINAL READING APPROVALS

of the thesis submitted by

Patrick Kyle Schwartz

Thesis Title: Investigating Soluble Organic Compounds in Aqueously Altered Carbonaceous Chondrites by Ultrahigh Resolution Orbitrap Mass Spectrometry

Date of Final Oral Examination: 14 June 2019

The following individuals read and discussed the thesis submitted by student Patrick Kyle Schwartz, and they evaluated his presentation and response to questions during the final oral examination. They found that the student passed the final oral examination.

Michael P. Callahan, Ph.D.	Chair, Supervisory Committee
Adam C. Colson, Ph.D.	Member, Supervisory Committee
Dale D. Russell, Ph.D.	Member, Supervisory Committee

The final reading approval of the thesis was granted by Michael P. Callahan, Ph.D., Chair of the Supervisory Committee. The thesis was approved by the Graduate College.

DEDICATION

I would like to dedicate this work to my friends and family; their support and encouragement is the unsung backbone of this work and the primary reason that the countless nights of bleary-eyed research came to fruition (finally) in such a fashion.

To my family, I hope that this work makes you proud and that it may serve as a reminder that the apple doesn't fall far from the tree. Regardless of whether you thought this work enjoyable and impressive or trivial and unpleasant, just know that you are, at least in part, responsible for this masterpiece or dumpster fire. Thank you for your endless love and support with all of my endeavors.

ACKNOWLEDGEMENTS

I would like to acknowledge Prof. Michael Callahan for his support throughout this process and beyond. I owe what I have learned as an analytical chemist primarily to his teachings and am very grateful for this opportunity. Also, I want to acknowledge Prof. Adam Colson and Prof. Dale Russell for reading my thesis and providing helpful comments during thesis committee meetings. Thank you to Dr. Xinzhu Pu for your help and guidance throughout this process. Thank you to my friends who have been by my side throughout this thesis, with a special thank you to Melissa Roberts and Shaun Millard for the constant sanity checks and all the fun over the last two years.

Support for this project was provided by the NASA Laboratory Analysis of Returned Samples (LARS) Program (Grant # NNX17AE51G). US Antarctic meteorite samples are recovered by the Antarctic Search for Meteorites (ANSMET) program which has been funded by NSF and NASA, and characterized and curated by the Department of Mineral Sciences of the Smithsonian Institution and Astromaterials Acquisition and Curation Office at NASA Johnson Space Center. Reflectance IR spectra of meteorites discussed in this thesis were publicly available via the Reflectance Experimental Laboratory at Brown University (RELAB).

ABSTRACT

Most meteorites are fragments from main-belt asteroids and contain extremely primitive materials that have preserved a compositional record of the early Solar System. After the formation of their parent bodies, carbonaceous chondrites experienced secondary modification from thermal metamorphism and/or aqueous alteration. Secondary processing likely influenced the synthesis and/or final composition of organic compounds in parent bodies; thus, these effects may be elucidated from the study of different meteorites. Although the role of aqueous alteration has been investigated for a few specific classes of compounds (such as amino acids), the effect of aqueous alteration on the full inventory of organic compounds in carbonaceous chondrites is still poorly understood.

I investigated the nature of soluble organic compounds in a full range of aqueously altered CM chondrites by electrospray ionization ultrahigh resolution orbitrap mass spectrometry. I determined that soluble organic composition was relatively consistent in CM chondrites despite varying degrees of aqueous alteration on the parent body/bodies; however, additional thermal metamorphism did show an extreme depletion in the organics identified. Additionally, I estimated the degree of aqueous alteration for CM chondrites that did not have a numerical degree of aqueous alteration via comparison of identified organics (although these estimates would need further verification). Finally, I observed that the position of the phyllosilicate-bound hydroxyl band in reflectance IR spectra of meteorites is related to the degree of aqueous alteration in meteorites. Organic-rich meteorites exhibited a maximum IR absorbance between 2.70 and 2.85 microns for the

phyllosilicate-bound hydroxyl band. This research has the potential to influence asteroid sample return missions, such as the current NASA OSIRIS-REx mission, by providing a more informative and accurate correlation of sample site to organic composition.

TABLE OF CONTENTS

LIST OF TABLES

LIST OF FIGURES

LIST OF ABBREVIATIONS

DBE	double bond equivalent
ESI	electrospray ionization
IOM	insoluble organic matter
IR	infrared spectroscopy
KMD	Kendrick mass defect
MeOH	methanol
MS	mass spectrometry
RELAB	NASA Reflectance Experimental Laboratory
SOM	soluble organic matter

CHAPTER ONE: BACKGROUND

Most meteorites are fragments from main-belt asteroids and contain extremely primitive materials that have preserved a compositional record of the early Solar System.[1] Carbonaceous chondrites are a class of carbon-rich meteorites that are composed primarily of fine-grained matrix, chondrules, and refractory inclusions.[2] There are nine known groups of carbonaceous chondrites: CM, CI, CV, CR, CH, CB, CK, CO, and C-ungrouped, each categorized based on bulk chemical and mineralogical composition.

Several groups of carbonaceous chondrites are known to contain organic compounds, which can be divided into two main types: soluble organic matter (SOM) and insoluble organic matter (IOM).[1,3,4] SOM comprises small (low molecular weight) organic compounds that can be extracted with typical aqueous and organic solvents. The carbonaceous chondrite group that contains the highest molecular complexity in the SOM is most likely CM chondrites, which may contain over a million different compounds based on the work of Schmitt-Kopplin et al.[5,6] Tens of thousands of unique molecular formulas representing four different general molecular classes (CHO, CHNO, CHOS, and CHNOS) were identified in the Murchison meteorite using Fourier-transform ion cyclotron resonance mass spectrometry.[5]

After the formation of their parent bodies, carbonaceous chondrites experienced secondary modification from thermal metamorphism and/or aqueous alteration. Thermal metamorphism was caused by various heating events, such as shockwave heating (impact-

associated), gravitational compression, and radioactive decay, and resulted in anhydrous minerals.[2,7] Aqueous alteration was caused by reactions with water and resulted in hydrous minerals. When assessing the extent of secondary processing, there is a petrographic scale from 1-6, where types 1-2 represent meteorites that have experienced different degrees of aqueous alteration (1 being most aqueously altered) and types 3-6 reflect thermal metamorphism (6 being the most thermally metamorphosed).[7] Furthermore, multiple research groups have developed diagnostic techniques to more finely assess the aqueous alteration scale such as the work by Browning et al., Rubin et al., and Alexander et al.[8–10] For example, Alexander et al. identified that aqueous altered meteorites could be easily classified based on the degree of hydration (wt.% H in water and OH). This scale ranges from 1.0 - 3.0 using 0.1 increments, and goes beyond assigning CM chondrites to simply CM1 or CM2 subgroups.[10]

Secondary processing likely influenced the synthesis and/or final composition of organic compounds in parent bodies; thus, these effects may be elucidated from the study of different meteorites. The effect of aqueous alteration on specific classes of organic compounds has been documented, such as the work by Glavin et al. where they determined that amino acid abundances were lower in the more-aqueously altered CM1 chondrites compared to CM2 chondrites.[11] Furthermore, these authors hypothesized that enantiomeric enrichment of L-isovaline and other α-dialkyl amino acids were due to aqueous alteration on the parent body.[11] Although the role of aqueous alteration has been investigated for a few specific classes of compounds (such as amino acids), the effect of aqueous alteration on the full inventory of organic compounds in carbonaceous chondrites is still poorly understood.[12] For example, how does the soluble organic composition in CM chondrites

change with increasing aqueous alteration? Are there any soluble organics that are common to all CM chondrites regardless of the degree of aqueous alteration? Do CM chondrites that have experienced very similar degrees of aqueous alteration have the same distribution and abundance of soluble organic compounds?

In this thesis, I investigated the nature of soluble organic compounds in a full range of aqueously altered CM chondrites by electrospray ionization ultrahigh resolution orbitrap mass spectrometry. ESI is a soft ionization technique suitable for more polar molecules (such as compounds containing N, S, and O), and results in little to no fragmentation.[13–15] Thus, mass peaks in an ESI mass spectrum usually represent parent ions. In positive ion mode, ESI generates positive ions of basic compounds by protonation ($[M+H]^+$) and/or by adduct formation (e.g., $[M+Na]^+$, $[M+K]^+$).[16,17] The generation of molecular formulas from accurate mass measurements is tied to both the accuracy of the mass spectrometer as well as its mass resolution. Mass resolution is the ability to separate two peaks in the mass spectrum and is defined as $m/\Delta m$ (at full-width at half-maximum). The orbitrap mass spectrometer is capable of ultrahigh mass resolution with a resolving power of 140,000 at *m/z* 200. For highly complex samples, ultrahigh resolution is required for resolving different mass peaks and to enable accurate mass measurements. While the orbitrap mass spectrometers cannot capture the level of molecular information compared to Fourier-transform ion cyclotron resonance mass spectrometers, the orbitrap is still very capable for the analysis of highly complex natural samples and sufficient for determination of unique molecular formulas of organic compounds with masses <600 Da.[18] A single mass spectrum at ultrahigh mass resolution provides tremendous amount of molecular-level information regarding the soluble organic composition of meteorites. Since ESI-MS response of

analytes are determined by multiple factors (not just solution concentration), abundances could not be determined in this thesis because it would require a seemingly endless supply of reference standard (the vast majority are not commercially available). Instead, I used data processing software to understand how the composition of soluble organic compounds changes with increasing aqueous alteration (and added thermal alteration in some meteorites). In this thesis, I used the scale by Alexander et al. to assess the degree of alteration in meteorites.[10]

Kendrick mass defect (KMD) analysis was used to help visualize and simplify the data produced. First, the experimental mass is converted to a Kendrick mass, see Eq. 1. In this work, CH_2 was used to produce Kendrick mass values by multiplying the experimental mass by the nominal mass of CH_2 (14.00000) and dividing by the exact mass of CH_2 (14.01565). [19,20]

$$\mathrm{KM} = \mathrm{mass}_{\mathrm{experimental}} \times \left[\frac{14.00000}{14.01565}\right] \quad (1)$$

where KM is the Kendrick mass. Subtracting the Kendrick mass from the nominal (integer) Kendrick mass produces a Kendrick mass defect, Eq. 2, which is identical for all compounds of identical heteroatom content and double bond equivalents.

$$\mathrm{KMD} = \mathrm{KM}_{\mathrm{nominal}} - \mathrm{KM} \quad (2)$$

A typical plot has the bounds KMD vs. Kendrick Mass ($KM_{nominal}$), where data points that fall into a horizontal line would be identified as belonging to a homologous series (in this case, increasing in alkylation).

It is important to point out that the terrestrial locations that carbonaceous chondrites can be found vary wildly in climate, and thus the amount of terrestrial contamination that they are exposed to varies as well. All of the meteorites analyzed in this thesis were

collected from Antarctica, as these samples have shown to be the least contaminated.[21] Lastly, it must be noted that while the majority of samples analyzed in this study were CM chondrites, each meteorite has experienced terrestrial weathering. The weathering grade of each meteorite is listed in **Table 1** and details the amount of rust and/or evaporate minerals present, which are indicators of terrestrial weathering. Data on meteoritic organic compounds was cross-checked with the weathering grade to ensure trends established in this work were not due to terrestrial weathering effects.

Asteroid Sample Return

While the study of meteorites provides some insight into the nature and distribution of organic material in asteroids, collection of uncontaminated material through direct sampling of asteroids would be more advantageous. The Origins, Spectral Interpretation, Resource Identification, and Security-Regolith Explorer (OSIRIS-REx) is NASA's first asteroid sample return mission, which aims to retrieve a surface sample directly from Bennu, an asteroid believed to be rich in organic material.[22] From previous Earth-based reflectance spectra, Bennu has been classified as a B-type asteroid and thought to be similar to CI and CM chondrites, indicating aqueous alteration was likely.[23–26]

Following a brief period of orbit, the spacecraft will obtain IR spectra of the surface using the OSIRIS-REx Visible and Infrared Spectrometer (OVIRS) with the purpose of assisting in the selection of an ideal sampling site on Bennu.[27] Special attention will be focused on the 2.9 - 3.6 μm spectral region, which corresponds to an IR range involved with vibrational excitations of organic molecules; however, only very limited information regarding organic composition can be gathered from these measurements. From reflectance IR spectra of carbonaceous chondrites, the IR band at 3.4 μm (2941 cm^{-1}; sp^3 C-H

stretching vibration) is typically used to indicate the presence of alkyl-organic compounds; however, it is often weak and does not inform on the complex distribution of soluble organic compounds in carbonaceous chondrites.

Alternatively, there is a strong IR band between 2.7 - 3.0 μm (3704 - 3333 cm^{-1}) that represents the phyllosilicate-bound hydroxyl groups.[28,29] We hypothesize that this IR band between 2.7 - 3.0 μm in the reflectance IR spectra of carbonaceous chondrites can be used to predict the relative abundance and type of organics present if there is a relationship between IR bands and the extent of aqueous alteration based on the scale of Alexander et al. Otherwise, we postulate that once OVIRS spectra of Bennu regolith can be fitted to the most spectrally similar chondritic meteorite samples, we can provide molecular-level data of Bennu analogs assuming they are among the meteorites analyzed in this thesis. These data may greatly assist in the selection of a sample site(s) that has the highest science return for the OSIRIS-REx mission as well as other future asteroid sample return missions. Furthermore, this characterization technique could be used to provide detailed information in extraterrestrial small bodies, specifically regarding their SOM inventory, without the need for sample recovery, leading to a very efficacious diagnostic tool for assessing potential organic delivery.

CHAPTER TWO: EXPERIMENTAL

2.1 Sample Handling/Meteorites Preparation

All sample handling tools (e.g. mortars, pestles, aluminum foil) and glassware were heated in an oven held at 500 ℃ for ~24 hours to remove any organic contamination. Meteorite samples were removed from their sample containers, photographed with an optical microscope, and then powdered with a ceramic mortar and pestle. Sample masses were weighed by difference using a Mettler Toledo XS64 analytical balance into baked-out ampules (2 mL). The meteorites analyzed in this study are listed in **Table 1** with their name (three-letter prefix shown, which abbreviates the geographic location from where the meteorite was recovered), designation regarding the specific fragment obtained, classification, and weathering grade.

2.2 Testing Sample Extraction Methods

Formic Acid Extraction with Desalting

The first method of sample preparation involved an extraction of the meteorite sample (100 mg ± 1 mg) with formic acid (1 mL, 98+%) in a flame-sealed ampule. The samples were then placed in an oven at 100 ℃ for 24 hours. Once cooled, the ampules were placed in sterile centrifuge tubes (15 mL) and centrifuged for 10 minutes. To open the ampules, the bottom portion of the ampules were frozen in liquid nitrogen and broken using ampule openers (Fisherbrand SafeSnap). Once thawed, ampules were placed in new, sterile centrifuge tubes (15 mL) and re-centrifuged. The supernatant was transferred with a pipette

to a tared and baked out test tube (13 mm). Solids that were left in the ampule were rinsed with 1 mL of formic acid, vortex-mixed, re-centrifuged, and the resulting supernatant was combined. This rinsing procedure was carried out twice to ensure the majority of soluble organic material that was extracted was transferred into the test tube. The sample extracts (now ~3 mL each) were placed in a vacuum centrifuge and dried overnight at room temperature to completely remove solvent.

For each sample, the dried residue was then reconstituted in 1% trifluoroacetic acid in water (300 μL) to desalt the samples prior to analysis, following instructions provided by Pierce for C18 pipette tip desalting. Next, the 100 μL C18 pipette tip was prepared by rinsing with 50:50 acetonitrile:water (100 μL, twice), followed by 0.1% TFA in water (100 μL, twice). The sample was then aspirated 30 times. The tip was rinsed with 0.1% TFA/5% acetonitrile (100 μL, twice) and the sample was eluted with 3-sequential, 100 μL rinses of 0.1% formic acid with varying acetonitrile:water concentrations of 50:50, 75:25, and 95:5, respectively. The resulting eluent was analyzed by ultrahigh resolution mass spectrometry in ESI (+) mode.

Formic Acid Extraction Without Desalting

One meteorite sample was also prepared without the desalting procedure. From the dried residue stage, the sample was reconstituted in 0.1% formic acid with varying acetonitrile:water concentrations of 50:50, 75:25, and 95:5, respectively (100 μL each, 300 μL total) to mimic the final solvent concentration from the desalting procedure above. The resulting solution was vortex-mixed and sonicated, transferred to an Eppendorf tube (2 mL) and centrifuged. A biphasic mixture was produced, where the top layer was a clear, yellow and the bottom layer was a cloudy, orange/brown (the latter subsequently clogged the ESI

infusion line). This was hypothesized as being due to excess salts being present after producing the dried residue, where the polarity of the solutions used for reconstitution led to a separation of layers. Both layers were analyzed separately by ultrahigh resolution mass spectrometry in ESI (+) mode.

Methanol Extraction

A simpler and faster approach was taken using less meteorite sample (50 mg $\pm$1 mg) and methanol (500 μL, Optima® LC/MS) as the extraction solvent. Additionally, methanol was shown by Schmitt-Kopplin to extract more soluble organics than any of the following solvents: ethanol, water, DMSO, acetonitrile, chloroform, and toluene.[5] Once added to an ampule, the samples were flame-sealed and heated in an oven at 100 ℃ for 24 hours. The ampules were opened and the sample was transferred with a Pasteur pipette to a 2-mL Eppendorf tube. Much of the original solid powder was transferred as well, so the samples were centrifuged and transferred again to a new 2-mL Eppendorf tube. This resulting solution was directly analyzed by ultrahigh resolution mass spectrometry in both ESI (+) and ESI (-) modes. *This extraction method was selected and applied to all meteorite samples in our study*.

Table 1: All 35 Meteorites Investigated in This Thesis

Name	Specific	Parent	Classification	Weathering*
ALH 83100	272	33	CM1/2	Be
ALH 84029	64	30	CM2	Ae
ALH 84033	41	9	CM2	Ae
ALH 84034	34	25	CM2	A
ALH 84042	25	19	CM2	A
ALH 84044	33	13	CM2	Ae
ALH 85013	65	23	CM2	A
DOM 03183	25	15	CM2	B
DOM 08003	14	9	CM2	B
EET 83355	39	9	C2 ungrouped	A/B
EET 87522	46	3	CM2	Be
EET 96016	16	0	CM2	Be
EET 96029	78	68	CM2	A/B
GRO 95566	36	11	CM (anomalous)	A/Be
LAP 02333	24	16	CM2	B
LEW 85311	74	24	CM (anomalous)	Be
LEW 85332	66	12	C3 ungrouped	B/C
LEW 87022	39	5	CM2	B
LEW 87148	25	0	CM2	Ae
LEW 88001	23	3	CM2	Ce
LEW 90500	79	2	CM2	B
LON 94101	107	8	CM2	Be
MAC 87300	80	27	C ungrouped	B
MAC 88100	55	46	CM2	Be
MAC 88107	67	8	C ungrouped	Be
MAC 88176	23	10	CM2	Be
MET 01070	48	0	CM1	Be
MIL 07700	37	28	CM2	A
PCA 02012	25	3	CM2	B
PCA 91008	46	40	CM (anomalous)	B
QUE 97990	54	0	CM2	Be
QUE 99038	28	20	CM (anomalous)	A/B
SCO 06043	25	0	CM1	B/Ce
TIL 91722	13	0	CM2	B/Ce
WIS 91600	61	59	CM (anomalous)	A/Be

*Weathering information obtained from Antarctic Meteorite Classification Database on NASA Johnson Space Center's curation website and is described as follows. A: Minor rustiness; rust haloes on metal particles and rust stains along fractures are minor. B: Moderate rustiness; large rust haloes occur on metal particles and rust stains on internal fractures are extensive. C: Severe rustiness; metal particles have been mostly stained by rust throughout. e: Evaporate minerals visible to the naked eye.

2.3 Mass Spectrometry Parameters

The orbitrap mass spectrometer used in this study is ideal for an analysis of complex organic samples, such as those presented here. The instrument generates an electric field between an inner and outer electrode that acts on the incoming ionized molecules differently based on each ion's generated electric field, which is dependent on the mass of each ion. The movement of charged species generates an image current that is detected and Fourier-transformed into a resulting m/z value. The benefits to this specific mass analyzer are due to both a high mass resolution and mass accuracy at which m/z values are detected.[30] A highly-resolved mass spectrum allows for peaks very close in m/z to be distinguished as individual peaks and high mass accuracy allows for near-exact identification of a peak's m/z value. The latter is essential to this analysis because molecular formulas can be calculated for peaks solely based on m/z values, assuming a mass spectrometer (like the orbitrap used here) can provide such detailed information.

Samples were analyzed using direct infusion at 10 μL/min into a Thermo Scientific Exactive Plus Orbitrap mass spectrometer equipped with an electrospray ionization source. A Pierce LTQ Velos ESI Positive Ion Calibration Solution was used to calibrate the instrument in ESI (+) mode, which resulted in mass error routinely below 1 ppm. Similarly, a Pierce ESI Negative Ion Calibration Solution was used prior to ESI (-) analyses, where mass error was usually below 2 ppm. Typical parameters for the mass spectrometer are shown in **Table 2.**

Table 2: Orbitrap Instrument Parameters

Parameter	ESI (+)	ESI (-)
Scan range	*m/z* 100-600	*m/z* 100-600
Resolution	140,000	140,000
Sheath gas flow rate	6-8 psi	10 psi
Aux gas flow rate	0 psi	1-2 psi
Spray voltage	2.80 kV	2.30 kV
Capillary temp.	240 ℃	240 ℃
S-lens RF level	50	50
Aux gas heater temp.	30 ℃	30 ℃

The syringe and infusion line were initially rinsed with 500 μL of methanol, followed by 500 μL of 1:1 MeOH:H_2O. The ESI (+) samples were analyzed twice to ensure reliability in data replication; ESI (-) samples were analyzed once due to limited remaining sample volume. Both the spray cone and stainless steel ion transfer capillary were cleaned between the analysis of ESI (+) and ESI (-), using a sonication procedure in methanol, 1:1 MeOH:H_2O, and water, sequentially, for 20 minutes per solution. While collecting mass spectra for ESI (+), the first run for each sample was compiled of 1,000 scans/sample and the second run averaged 500 scans/sample. ESI (-) used an average of 500 scans/sample.

2.4 Data Analysis

Data analysis was performed using software designed for petroleomics. For both ESI (+) and ESI (-) spectra, the mass accuracy was set at 2 ppm with a minimum abundance threshold of 0.02% of the base peak from m/z 100-600. A double bond equivalent (DBE) limit was set from 0-40 and four passes were made to identify molecular classes; the possible elements were increased as described in **Table 3** with each sequential pass. For Orbitrap mass spectra, generally a constant peak width of 0.005 Da is appropriate. Also, mass spectra were collected for a procedural blank (methanol) in ESI (+) and ESI (-), respectively, and were used to background subtract from the sample spectra.

Table 3: Elements used for series identification, in the order they were applied

Pass	1	2	3	4
C	0-200	0-200	0-200	0-200
H	0-1000	0-1000	0-1000	0-1000
O	-	0-20	-	0-20
N	-	-	0-20	0-20
S	-	-	-	0-5

The software uses mass accuracy in two ways: first, when calculating *de novo* compositions used to initiate assignment of a new class and second, when extending the *de novo* assignments by CH_2 and H_2 differences. In the first case, only those compositions within +/- the ppm tolerance of the target peak are allowed, and in the second case, any peak considered for matching by series extension must be within +/- the ppm tolerance of the "anchor" peak from which the extension is being tried. The maximum *de novo* mass used for identifying molecular classes was set at 250 m/z. A peak can have only one monoisotopic species assigned to it, but it could have more than one higher isotopic species assigned, which attempts to account for the fact that with higher isotopes, it is possible to have multiple unresolved peaks that appear as one when centroided. The software's algorithm relaxes the one assignment per peak rule and allows a peak to be assigned to more than one non-monoisotopic composition, which can also lead to the total assigned abundance to sum to more than 100% if there are a lot of these multiple assignments.

The percentage is calculated by summing the abundances of the assignments at that level (Class or DBE) and dividing by the total assigned abundance. It is also important to note that percentages are completely non-quantitative since they are based on abundance only and do not take into account differences in ionization or detection efficiency based on composition or m/z. Additionally, when the resulting molecular formulas are compared by percentage this does not represent the abundance of these compounds within the meteorite

sample. This is due to variations in ionization efficiency as some compounds are more likely to become charged (and thus detectable) than others. However, comparing the same classes of compounds across different meteorites gives more information regarding relative abundance, as it can be assumed that identical compounds in different meteorite samples will still have identical ionization efficiency.

Ultrahigh resolution orbitrap mass spectra revealed the presence of numerous homologous series of molecules, which were identifiable by regular intervals between peaks that correspond to $–CH_2–$ groups (alkylation). In addition, regular intervals between peaks differing in degree of saturation (H_2) were also commonly observed.

CHAPTER THREE: RESULTS

Both positive ion and negative ion ultrahigh resolution mass spectra were acquired for methanol extracts of 35 different meteorite samples. In this thesis, only positive ion data will be discussed. **Figure 1** shows mass spectra from four different meteorite samples, which are representative of meteorites that experienced varying degrees of aqueous alteration and in one case, additional thermal alteration. These mass spectra *were produced by including only compounds assigned to molecular formulas* using the petroleomics software and, therefore, do not show all of the peaks actually measured in the originally acquired mass spectrum. The resulting mass spectra are still complex. For example, 1,138 molecular formulas were identified for TIL 91722, 1,452 molecular formulas were identified for LAP 02333, and 859 molecular formulas were identified for MET 01070, which are aqueously altered meteorites. For meteorites that have experienced additional thermal metamorphism, the number of identified organics was greatly reduced; for example, only 72 molecular formulas were identified in ALH 84033. As aqueous alteration increases from TIL 91722 (1.9) to MET 01070 (1.2), the centroid of the mass spectrum shifts from near *m/z* 200 to just below *m/z* 300.

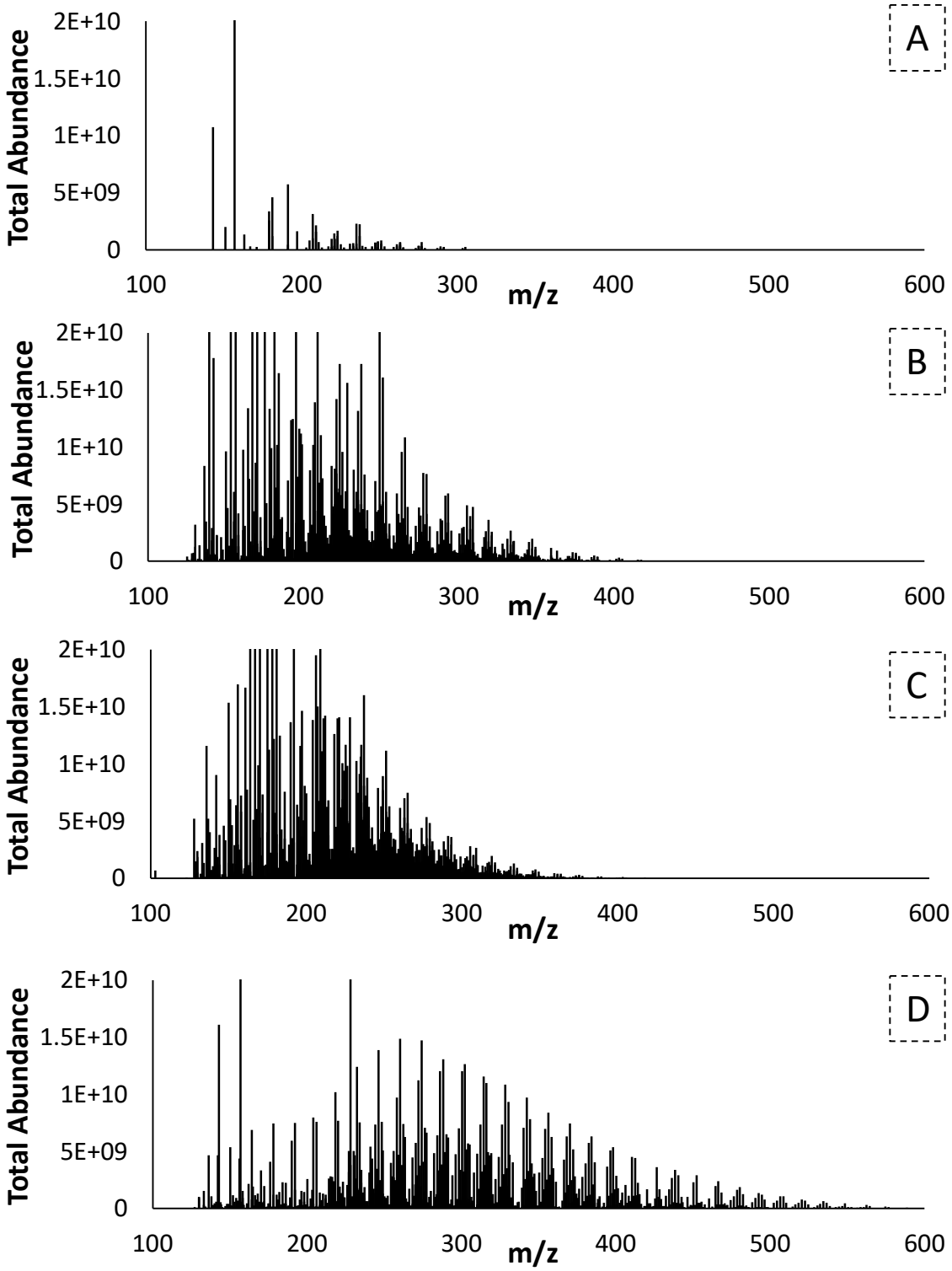

Figure 1: ESI (+) mass spectra generated from all identified molecular classes in four meteorites. (A) MIL 07700, 2.2 (B) TIL 91722, 1.9 (C) LAP 02333, 1.5 (D) MET 01070, 1.2. The three-letter, five-number code identifies the meteorite analyzed, where the number following is linked to the aqueous alteration experienced by the sample, identified from Alexander et al. (2012).

For aqueously altered CM chondrites, a closer examination of the ultrahigh resolution mass spectra reveal the presence of numerous distinct homologous series of compounds, which can be defined according to "class" (i.e. numbers of heteroatoms), "type" (i.e. number of double bond equivalents; mass spacing of ~2 Da indicating change in degree of saturation) and "carbon distribution" (repeating mass spacing pattern of ~14 Da for $(-CH_2-)_n$ groups). To illustrate an example, **Figure 2** shows all compounds belonging to all of the identified series in TIL 91722, all compounds belonging to the C_xH_yN, series across all DBE, and also shows one homologous series of the same class and same type, but different carbon distribution (repeating mass spacing pattern of ~14 Da). The molecular complexity and variation in class, type, and carbon distribution is reminiscent of humic/fulvic acid and petroleum, the latter typically containing numerous organic compounds with a single nitrogen atom, however, molecular diversity within and across chemical classes is generally accepted as evidence of extraterrestrial/meteoritic chemistry.[31,32]

Across a majority of the meteorites, 10 molecular classes of interest were identified. In **Table 4**, each box reports a percentage for a specific molecular class, which was calculated by summing the intensity of detected molecular formulas belonging a specific class and dividing by the intensity of all identified molecular formulas. These 10 molecular classes composed ~87% of all organics identified in meteorite samples (excluding the thermally-altered meteorites, which lacked a large portion of organics compared to aqueously altered meteorites). Within the C_xH_yN class of compounds, the percentage appeared to increase with meteorites that have experienced greater degrees of aqueous alteration.

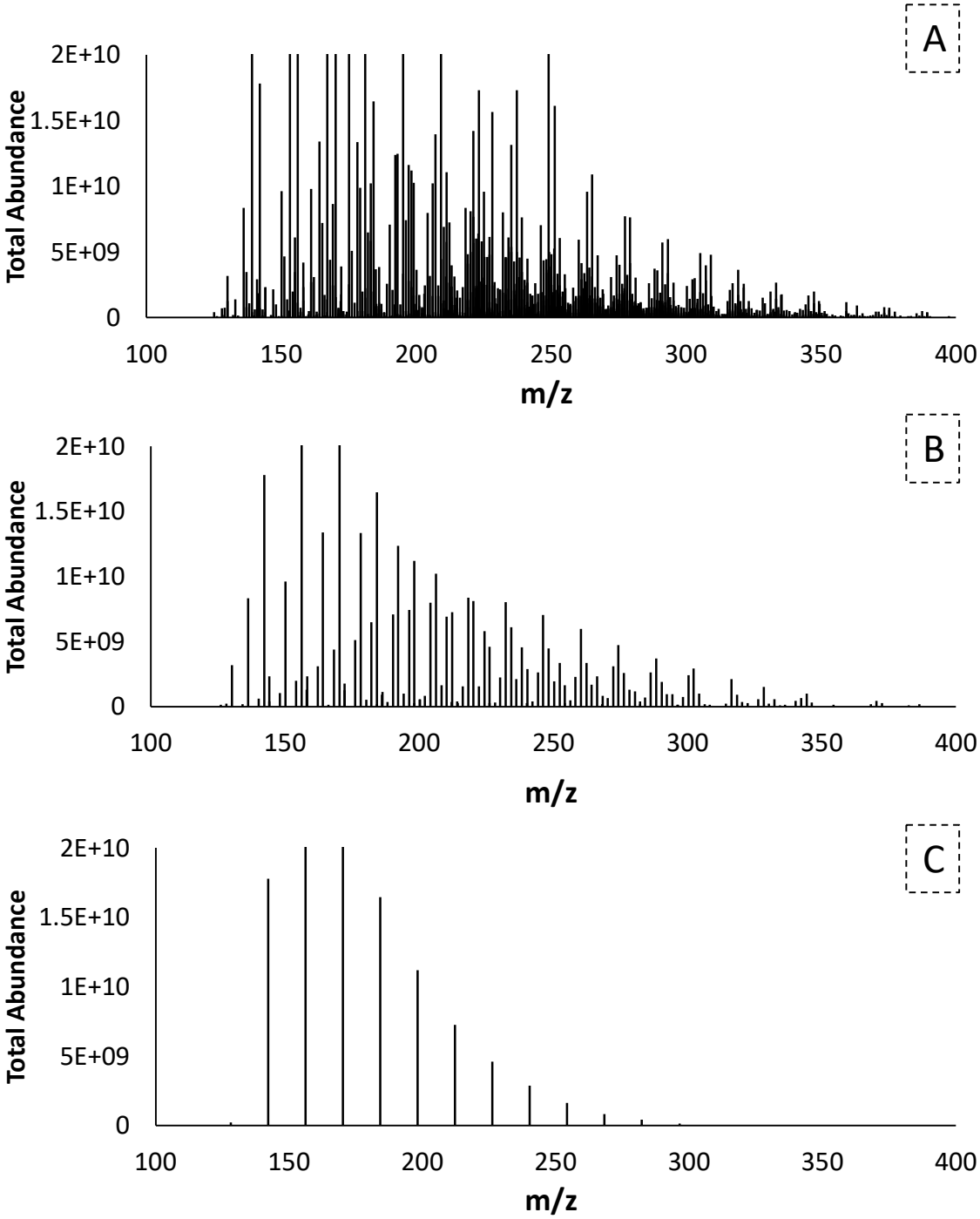

Figure 2: Mass spectra of TIL 91722 further analyzed to highlight the complexity of the samples analyzed. (A) All peaks belonging to all identified classes. (B) All peaks identified within the C_xH_yN class, regardless of type. (C) Homologous series of peaks with base formula of $C_7H_{15}N$, identical type, and distinct carbon distribution (increase of CH_2 units).

Interestingly, it may be possible to use C_xH_yN and $C_xH_yN_2$ percentages as a method to identify whether meteorites have undergone thermal metamorphism and/or the extent of aqueous alteration based on trends observed in our set of 35 meteorites. For example, MAC 88100 was given an aqueous alteration value of 1.8, indicating it is less aqueous altered. Through our analysis of this sample, it was found that both C_xH_yN % and $C_xH_yN_2$ % were both 0%. This would suggest that MAC 88100 has undergone some sort of late-stage thermal alteration, such as shockwave heating. Conversely, DOM 03183 has an aqueous alteration value of 1.6 and was previously thought to have possibly experienced thermal metamorphism, however based on its C_xH_yN % and $C_xH_yN_2$ % of 61.38% and 16.90%, respectively, would indicate that the meteorite likely hasn't experienced any significant heating event.

For meteorites listed below DOM 08003 (1.1) in **Table 4**, Alexander et al. had not identified a numerical degree of aqueous alteration associated with these meteorites, but based on our observations of molecular class %, we would classify these meteorites as thermally altered (2.0 or higher) with the exception of LEW 85332. LEW 85332 was observed to be similar in organic composition to LEW 88001, possibly indicating similarities to a value of 1.6. All other molecular classes seem fairly independent of aqueous alteration and remain in a consistent range.

Table 4: Meteorite series heatmap. This table correlates all meteorites analyzed (rows) with the 10 most detected heteroatom classes (columns).

C_xH_yR =	N	N_2	N_6O	N_6	NO	NO_7	N_6O_2	O_8	N_2O	NO_8
EET 83355 (2.4)	0.00	0.00	47.70	31.84	0.00	0.00	9.91	0.00	0.00	0.00
MIL 07700 (2.2)	0.00	0.00	35.47	21.52	0.00	0.00	13.30	0.00	0.00	0.00
ALH 84033 (2.1)	0.00	0.00	0.00	0.00	5.04	0.00	0.00	7.66	0.00	16.85
EET 87522 (2.0)	0.00	0.00	0.00	0.00	0.00	34.09	36.55	14.72	0.00	0.96
PCA 91008 (2.0)	0.00	0.00	0.28	0.00	0.00	17.08	0.00	12.73	0.00	28.73
EET 96029 (1.9)	1.76	0.00	0.00	0.00	0.00	13.16	1.97	13.24	0.00	1.87
LEW 85311 (1.9)	20.29	30.18	4.65	3.04	7.91	1.23	2.32	3.07	6.68	0.65
TIL 91722 (1.9)	18.79	31.84	4.34	4.92	4.69	0.92	2.15	0.06	7.37	0.04
LON 94101 (1.8)	35.65	15.10	8.35	6.60	9.23	2.77	3.70	3.10	2.98	0.19
MAC 88100 (1.7)	0.00	0.00	0.00	0.00	5.11	0.00	0.00	3.91	0.00	31.88
QUE 97990 (1.7)	18.74	10.90	11.09	9.87	9.67	2.75	6.15	1.80	4.25	0.29
DOM 03183 (1.6)	61.38	16.90	0.09	0.11	6.29	0.96	0.78	1.57	0.59	0.05
GRO 95566 (1.6)	21.98	36.99	2.98	3.55	4.99	1.84	1.40	0.41	4.48	0.09
LEW 88001 (1.6)	26.33	20.97	3.33	3.81	11.52	5.54	1.88	4.04	6.60	0.76
LEW 90500 (1.6)	44.78	29.35	0.86	0.52	9.37	1.31	0.71	0.94	5.41	0.28
LAP 02333 (1.5)	25.83	24.21	5.29	6.13	10.13	1.00	2.34	1.33	7.28	0.24
ALH 85013 (1.4)	24.03	15.86	5.51	6.92	10.89	2.25	4.28	2.21	6.13	0.67
EET 96016 (1.4)	32.68	31.06	1.84	6.34	6.55	2.28	0.80	1.97	5.92	0.51
LEW 87022 (1.4)	37.40	15.79	9.04	5.42	7.28	3.98	4.23	1.32	2.10	0.20
MAC 88176 (1.4)	55.74	24.18	0.25	0.12	6.31	5.25	0.39	0.80	2.89	0.22
LEW 87148 (1.3)	36.64	43.48	0.36	0.04	5.80	1.15	0.09	0.58	6.23	0.00
ALH 84029 (1.2)	42.47	25.03	5.22	3.39	6.98	1.65	2.63	1.00	3.32	0.11
ALH 84042 (1.2)	27.23	6.77	11.09	10.97	6.94	13.59	5.35	1.56	1.05	2.29
ALH 84044 (1.2)	55.68	23.42	1.30	1.24	6.81	0.00	1.65	0.96	2.53	0.00
MET 01070 (1.2)	49.03	16.16	2.77	1.03	7.70	4.69	0.36	2.25	0.50	0.59
SCO 06043 (1.2)	38.57	17.00	0.74	0.00	14.66	9.09	0.00	4.96	0.71	1.08
ALH 83100 (1.1)	37.24	7.79	6.99	4.98	12.94	0.00	8.99	3.32	1.06	0.00
ALH 84034 (1.1)	45.97	19.75	2.71	3.76	6.47	8.85	1.97	1.22	3.46	0.00
DOM 08003 (1.1)	32.18	39.97	0.75	0.57	7.78	1.63	0.78	0.83	7.11	0.36
LEW 85332	26.02	15.47	14.71	20.60	4.59	0.00	1.44	0.00	3.65	0.00
MAC 87300	0.00	0.00	23.67	9.36	0.00	0.00	13.33	8.21	0.00	3.03
MAC 88107	2.80	0.00	3.26	0.70	0.00	0.00	1.15	0.00	0.00	0.00
PCA 02012	0.00	0.00	0.00	0.00	0.00	0.00	0.00	5.78	0.00	0.00
QUE 99038	0.00	0.00	0.00	0.00	0.00	32.99	0.00	0.00	0.00	1.10
WIS 91600	0.99	0.00	36.28	25.98	0.00	6.05	18.33	4.24	0.00	0.00

Along with comparing meteorites based on their total class percentage, the meteorites were also scrutinized at the molecular level to identify if there were changes present that may have been overlooked. To do this Kendrick mass defect plots were generated for each sample. A standard Kendrick mass defect plot can be used to identify compounds present within a homologous series that have increasing alkylation. This provides a more detailed picture of the organics present. Sample Kendrick mass defect plots for TIL 91722, LAP 02333, and MET 01070, **Figures 3-5** respectively, highlight molecular level information for the C_xH_yN class of compounds. The tables found below each Kendrick plot show the molecular formula that each dot represents, as well as the base formula and DBE associated. Both TIL 91722 and LAP 02333 have similar composition within the C_xH_yN class, while MET 01070 is much more robust in both type and carbon distribution. This study identified that as aqueous alteration increases in the meteorite, it appears that the carbon number increases for the C_xH_yN class. This result leads us to believe that aqueous alteration potentially played a role in these larger compounds formation or perhaps extended their longevity compared to more primitive meteorite samples. Additional Kendrick mass defect plots can be found in Appendix A, which show all the molecular compounds identified for each meteorite.

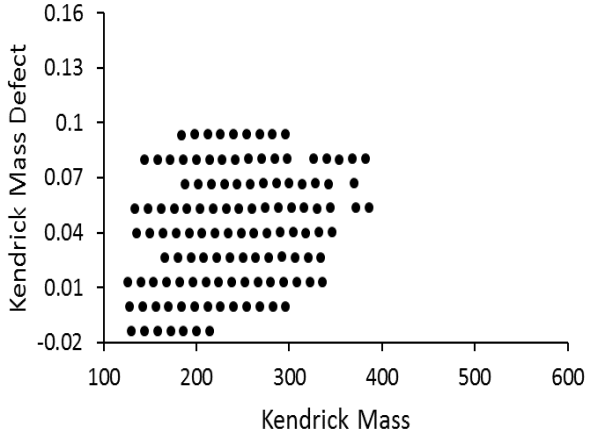

TIL 91722	Carbon Number (C_x)																				
Molecular Formula	8	9	10	11	12	13	14	15	16	17	18	19	20	21	22	23	24	25	26	27	**DBE**
$C_xH_{(2x-13)}N$																					**8**
$C_xH_{(2x-11)}N$																					**7**
$C_xH_{(2x-9)}N$																					**6**
$C_xH_{(2x-7)}N$																					**5**
$C_xH_{(2x-5)}N$																					**4**
$C_xH_{(2x-3)}N$																					**3**
$C_xH_{(2x-1)}N$																					**2**
$C_xH_{(2x+1)}N$																					**1**
$C_xH_{(2x+3)}N$																					**0**

Figure 3: Kendrick mass defect plot for TIL 91722 within the CHN class. Each dot represents a unique molecular formula and the table details each molecular formula, where a green box indicates an observed compound and a dark gray box indicates a molecule missing in series from a certain "type" or DBE. White boxes were formulas not observed.

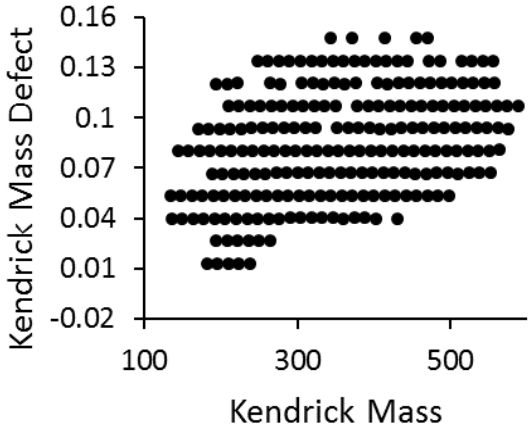

MET 01070	Carbon Number (C_x)																																
Molecular Formula	9	10	11	12	13	14	15	16	17	18	19	20	21	22	23	24	25	26	27	28	29	30	31	32	33	34	35	36	37	38	39	40	41	42	DBE
$C_xH_{(2x-21)}N$																																			12
$C_xH_{(2x-19)}N$																																			11
$C_xH_{(2x-17)}N$																																			10
$C_xH_{(2x-15)}N$																																			9
$C_xH_{(2x-13)}N$																																			8
$C_xH_{(2x-11)}N$																																			7
$C_xH_{(2x-9)}N$																																			6
$C_xH_{(2x-7)}N$																																			5
$C_xH_{(2x-5)}N$																																			4
$C_xH_{(2x-3)}N$																																			3
$C_xH_{(2x-1)}N$																																			2

Figure 4: Kendrick mass defect plot for MET 01070 within the CHN class. Each dot represents a unique molecular formula and the table details each molecular formula, where a green box indicates an observed compound and a dark gray box indicates a molecule missing in series from a certain "type" or DBE. White boxes were formulas not observed.

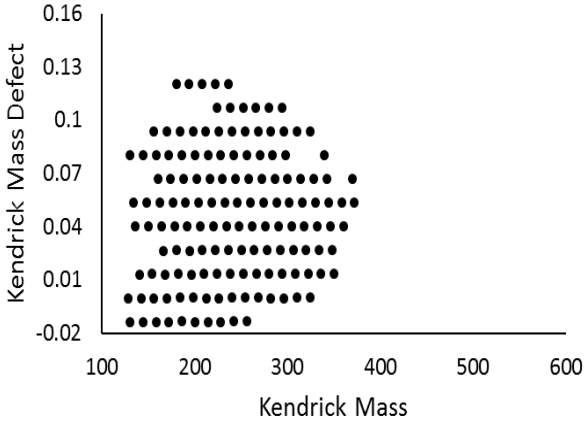

LAP 02333	Carbon Number (C_x)																			
Molecular Formula	8	9	10	11	12	13	14	15	16	17	18	19	20	21	22	23	24	25	26	DBE
$C_xH_{(2x-17)}N$																				10
$C_xH_{(2x-15)}N$																				9
$C_xH_{(2x-13)}N$																				8
$C_xH_{(2x-11)}N$																				7
$C_xH_{(2x-9)}N$																				6
$C_xH_{(2x-7)}N$																				5
$C_xH_{(2x-5)}N$																				4
$C_xH_{(2x-3)}N$																				3
$C_xH_{(2x-1)}N$																				2
$C_xH_{(2x+1)}N$																				1
$C_xH_{(2x+3)}N$																				0

Figure 5: Kendrick mass defect plot for LAP 02333 within the CHN class. Each dot represents a unique molecular formula and the table details each molecular formula, where a green box indicates an observed compound and a dark gray box indicates a molecule missing in series from a certain "type" or DBE. White boxes were formulas not observed.

Due to the observation of molecular weight seeming to increase with increasing aqueous alteration, the resulting lists of molecular formulas for each meteorite were analyzed to determine what effect (if any) aqueous alteration played on double bond equivalents (DBE) and carbon number, see **Figure 6**. It appears that all unheated meteorites vary from an average DBE of ~4-7 and an average carbon number of ~10-20, with no observed trend with the degree of aqueous alteration. Most thermally altered meteorites were easily identified due to their low average carbon number in the organics identified. DOM 03183, while previously identified as "possibly heated", showed average DBE and average carbon number values on the high end of the unheated meteorites, while the majority of heated meteorites had DBE values that varied from ~1-10 and carbon number values of ~4-12. Furthermore, DOM 03183 was relatively organic-rich, leading us to believe that it did not experience a significant degree of thermal metamorphism or shock. For the C, C_2, and C_3-ungrouped meteorites, both MAC 87300, MAC 88107, and EET 83355 were relatively organic-poor and more similar to thermally metamorphosed CMs.

For this thesis research to be applicable towards remote probing of organics, a correlation to infrared spectroscopy (IR) must be made, as it is the primary instrument used in OSIRIS-REx to recognize the presence of organics and assist with the selection of a sampling site(s). Many meteorites analyzed in this thesis had reflectance IR spectra freely available from the Reflectance Experiment Laboratory (RELAB) at Brown University.

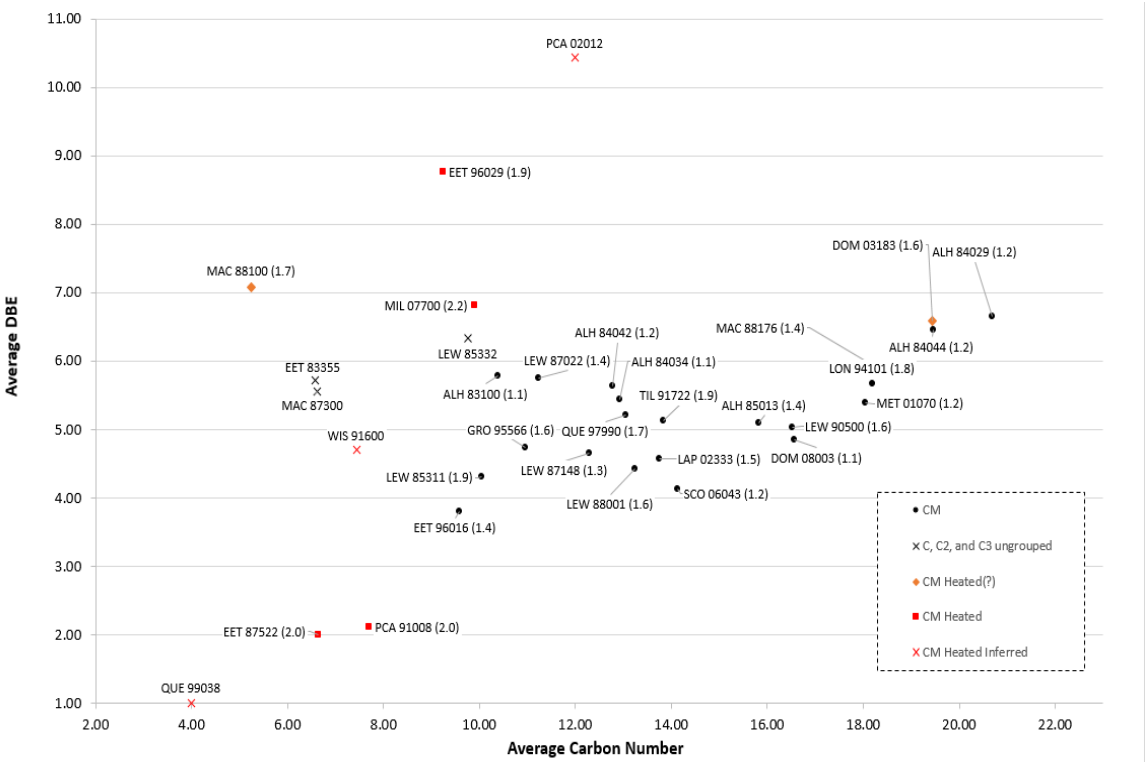

Figure 6: Correlates the average double bond equivalents across all molecular series identified per meteorite to the average carbon number across all molecular series. This was calculated from the molecular formulas generated upon analysis. Data label includes the meteorite name as well as the aqueous alteration value identified by Alexander et al. (2012) in parenthesis.

For the OSIRIS-REx asteroid sample return mission, the IR band at 3.4 μm, which corresponds to aliphatic compounds, is informative towards verifying the presence of organic compounds in the regolith. However, this band is relatively weak and difficult to identify due to the larger band located around 2.7-2.9 μm representing phyllosilicate-bound hydroxyl groups, which commonly obstructs some identifiable signal from the aliphatic bands because it is very broad. Also, the 3.4 μm band is not present in some meteorites, however, it was determined that the location of the hydroxyl band's minima could be used to assess whether or not the sample would be expected to contain organics, see **Figure 7**. Both TIL 91722 and LEW 88001 would not have been expected to be rich in organics due

to their lack of a 3.4 μm band; however, using their hydroxyl band location would suggest that there might be organics present in both samples. A band location between 2.7-2.85 μm would suggest the possibility of an organic rich sample, which was confirmed by our mass spectral data. There is a chance, as in the case for MAC 88100, that the hydroxyl band location would appear to represent an organic-rich sample, however, upon analysis this was determined to not be the case. Instead, MAC 88100 appears similar to a thermally-altered meteorite due to the limited organic inventory detected. This is considered a special case and the location of the hydroxyl band should be used in conjunction with an identified 3.4 μm band to assess the extent of organic composition.

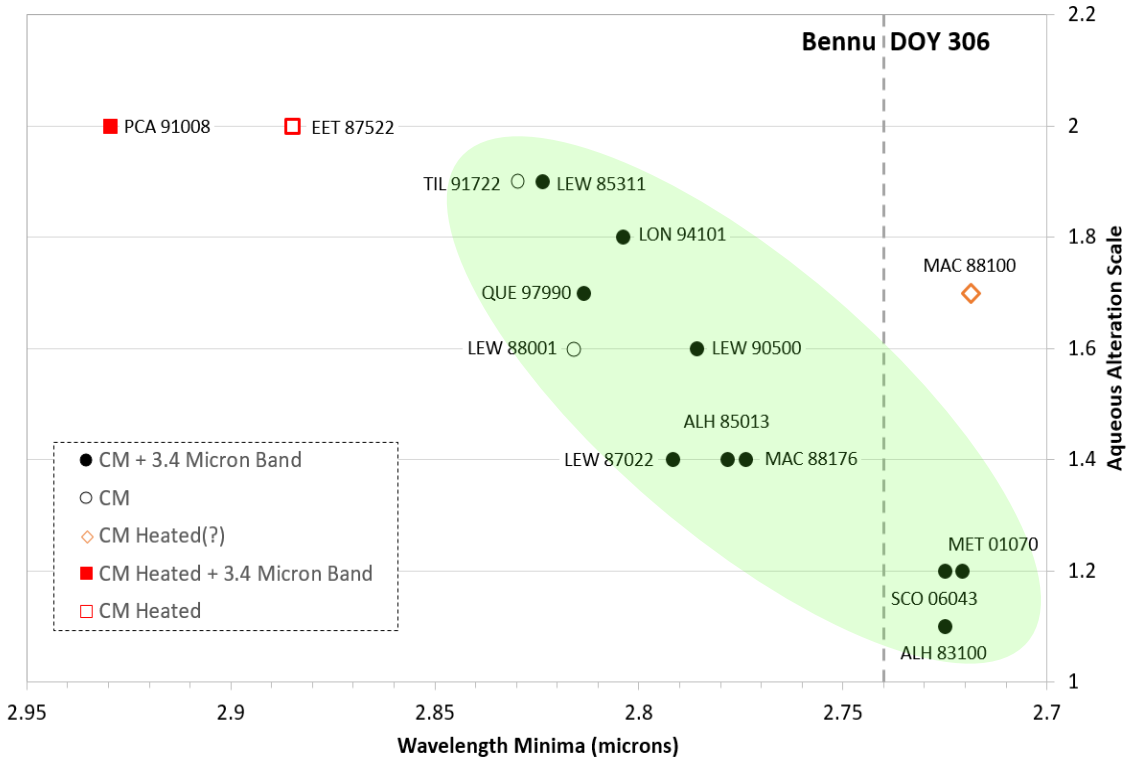

Figure 7: The degree of aqueous alteration as identified by Alexander et al. (2012) correlated to the location of the hydroxyl band of bonded water to phyllosilicates. Key identifies whether bands were present or absent at 3.4 microns, generally used for assessing aliphatic absorption.

The location of the hydroxyl band for asteroid Bennu (in spectrum DOY 306) sits at 2.74 μm, indicating a likelihood for similarities to the more aqueously altered meteorites, however the identification of a 3.4 μm band is somewhat obscured due to the nature of the long-range measurement.[33] If identifying organic bands continues to be ambiguous, then the use of this hydroxyl band correlation should be used to provide insight as to whether the sample site is organic-rich. This correlation could be used to assess sample sites and determine an optimal sampling location for this mission. It is important to note that this study pertained to CM chondrites and while there were a few chondrites of other groups present, additional work would need to be done to investigate the role aqueous alteration plays on the organic composition of other chondrites, such as CI and CR chondrites.

Final Remarks

1. Aqueous alteration does not significantly affect the organic inventory within the SOM, while thermal metamorphism causes a significant reduction in the SOM.
2. There is a no observable change in the mass spectrum, nor in the identified molecular compounds, due to increasing aqueous alteration, possibly indicating that the SOM has all reacted under similar conditions, unaffected by slight variations in aqueous alteration.
3. We have identified 10 representative classes that can be used to assess the organic inventory of CM chondrites.
4. We observed that the average carbon number ranged from 10-20 and the average DBE ranged from 4-7 in aqueous altered CM chondrites.

5. Samples that have undergone thermal metamorphism are sporadic in their average DBE and average carbon number response, but for the most part, result in a lower carbon number than that of unheated chondrites.
6. IR measurements indicating the position of the hydroxyl band can be used to identify the degree of aqueous alteration. Furthermore, we investigated the relationship between degree of aqueous alteration and soluble organic composition. These correlations can be extended to small bodies such as Bennu for identification of organic-rich sites using only remote IR data. If a hydroxyl band located between 2.7 - 2.85 microns is observed by the OVIRS instrument, it would most likely represent an organic-rich sample. Additionally, the hydroxyl band is of much larger intensity than that of the 3.4-micron band currently used to identify organics, leading to an increased detection limit.
7. With this correlation, extraterrestrial small bodies of similar nature to asteroid Bennu can be remotely observed to predict their organic inventory without the need for direct sampling. Additionally, the data collected in this study has the potential to help scientists predict the organic composition of an asteroid surface simply from ground-based IR measurements.

REFERENCES

1. Sephton, M. A. Organic compounds in carbonaceous meteorites. Nat. Prod. Rep. 19, 292–311 (2002).

2. Braukmüller, N., Wombacher, F., Hezel, D. C., Escoube, R. & Münker, C. The chemical composition of carbonaceous chondrites: Implications for volatile element depletion, complementarity and alteration. Geochim. Cosmochim. Acta 239, 17–48 (2018).

3. Alexander, C. M. O. D., Cody, G. D., De Gregorio, B. T., Nittler, L. R. & Stroud, R. M. The nature, origin and modification of insoluble organic matter in chondrites, the major source of Earth's C and N. Chem Erde 77, 227–256 (2017).

4. Botta, O. & Bada, J. L. Extraterrestrial organic compounds in meteorites. Surv. Geophys. 23, 411–467 (2002).

5. Schmitt-Kopplin, P. et al. High molecular diversity of extraterrestrial organic matter in Murchison meteorite revealed 40 years after its fall. Proc. Natl. Acad. Sci. U. S. A. 107, 2763–2768 (2010).

6. Ehrenfreund, P., Glavin, D. P., Botta, O., Bada, J. L. & Cooper, G. Extraterrestrial amino acids in Orgueil and Ivuna: Tracing the parent body of CI type carbonaceous chondrites. Proc. Natl. Acad. Sci. U. S. A. 98, 2138–2141 (2001).

7. Huss, G. R., Rubin, A. E. & Grossman, J. N. Thermal Metamorphism in Chondrites. in Meteorites and the early solar system II 567–586 (1995).

8. Browning, L. B., McSween, H. Y. & Zolensky, M. E. Correlated alteration effects in CM carbonaceous chondrites. Geochim. Cosmochim. Acta 60, 2621–2633 (1996).

9. Rubin, A. E., Trigo-Rodrigues, J. M., Huber, H. & Wasson, J. T. Progressive aqueous alteration of CM carbonaceous chondrites. Geochim. Cosmochim. Acta 71, 2361–2382 (2007).

10. Alexander, C. M. O. D., Howard, K. T., Bowden, R. & Fogel, M. L. The classification of CM and CR chondrites using bulk H, C and N abundances and isotopic compositions. Geochim. Cosmochim. Acta 123, 244–260 (2013).

11. Glavin, D. P. & Dworkin, J. P. Enrichment of the amino acid L-isovaline by aqueous alteration on CI and CM meteorite parent bodies. Proc. Natl. Acad. Sci. U. S. A. 106, 5487–5492 (2009).

12. Botta, O., Martins, Z. & Ehrenfreund, P. Amino acids in Antarctic CM1 meteorites and their relationship to other carbonaceous chondrites. Meteorit. Planet. Sci. 42, 81–92 (2007).

13. Danger, G. et al. Characterization of laboratory analogs of interstellar/cometary organic residues using very high resolution mass spectrometry. Geochim. Cosmochim. Acta 118, 184–201 (2013).

14. Fenn, J. B., Mann, M., Meng, C. K., Wong, S. F. & Whitehouse, C. M. Electrospray ionization-principles and practice. Mass Spectrom. Rev. 9, 37–70 (1990).

15. Iribarne, J. V & Thomson, B. A. Charge and fission of droplets in electrostatic sprays. J. Chem. Phys. 64, 4977 (1976).

16. Kruve, A., Kaupmees, K., Liigand, J., Oss, M. & Leito, I. Sodium adduct formation efficiency in ESI source. J. Mass Spectrom. 48, 695–702 (2013).

17. Wang, K., Han, X., Gross, R. W. & Gokel, G. W. Direct Evidence for Arylmethyl Ether Coordination of Sodium and Potassium Cations: An Electrospray Ionization Mass Spectrometry Study. J. Am. Chem. Soc. 117, 7680–7686 (1995).

18. Remucal, C. K., Cory, R. M., Sander, M. & McNeill, K. Low Molecular Weight Components in an Aquatic Humic Substance As Characterized by Membrane Dialysis and Orbitrap Mass Spectrometry. Environ. Sci. Technol. 46, 9350–9359 (2012).

19. Fouquet, T. & Sato, H. Improving the Resolution of Kendrick Mass Defect Analysis for Polymer Ions with Fractional Base Units. Mass Spectrom. 6, A0055–A0055 (2017).

20. Hughey, C. A., Hendrickson, C. L., Rodgers, R. P., Marshall, A. G. & Qian, K. Kendrick Mass Defect Spectrum: A Compact Visual Analysis for Ultrahigh-Resolution Broadband Mass Spectra. Anal. Chem. 73, 4676–4681 (2001).

21. Naraoka, H., Shimoyama, A., Matsubaya, O. & Harada, K. Carbon isotopic compositions of Antarctic carbonaceous chondrites with relevance to the alteration and existence of organic matter. Geochem. J. 31, 155–168 (1997).

22. Gal-Edd, J. & Cheuvront, A. The OSIRIS-REx Asteroid Sample Return Mission operations design. in 2015 IEEE Aerospace Conference 1–9 (2015). doi:10.1109/AERO.2015.7118883

23. Lauretta, D. S. et al. OSIRIS-REx: Sample Return from Asteroid (101955) Bennu. Space Sci. Rev. 212, 925–984 (2017).

24. Clark, B. E. et al. Asteroid (101955) 1999 RQ36: Spectroscopy from 0.4 to 2.4 μm and meteorite analogs. Icarus 216, 462–475 (2011).

25. Emery, J. P. et al. Thermal infrared observations and thermophysical characterization of OSIRIS-REx target asteroid (101955) Bennu. Icarus 234, 17–35 (2014).

26. Alí-Lagoa, V. et al. Physical properties of B-type asteroids from WISE data. Astron. Astrophys. 1–16 (2013). doi:10.1051/0004-6361/201220680

27. Reuter, D. C. et al. The OSIRIS-REx Visible and InfraRed Spectrometer (OVIRS): Spectral Maps of the Asteroid Bennu. Space Sci. Rev. 214, (2018).

28. Osawa, T., Kagi, H., Nakamura, T. & Noguchi, T. Infrared spectroscopic taxonomy for carbonaceous chondrites from speciation of hydrous components. Meteorit. Planet. Sci. 40, 71–86 (2005).

29. McAdam, M. M., Sunshine, J. M., Howard, K. T. & McCoy, T. M. Aqueous alteration on asteroids: Linking the mineralogy and spectroscopy of CM and CI chondrites. Icarus 245, 320–332 (2015).

30. Zubarev, R. A. & Makarov, A. Orbitrap Mass Spectrometry. Anal. Chem. 85, 5288–5296 (2013).

31. Yamashita, Y. & Naraoka, H. Two homologous series of alkylpyridines in the Murchison meteorite. Geochem. J. 48, 519–525 (2014).

32. Naraoka, H., Yamashita, Y., Yamaguchi, M. & Orthous-Daunay, F. R. Molecular Evolution of N-Containing Cyclic Compounds in the Parent Body of the Murchison Meteorite. ACS Earth Sp. Chem 1, 540–550 (2017).

33. Hamilton, V. E. et al. Evidence for widespread hydrated minerals on asteroid (101955) Bennu. Nat. Astron. 3, 332–340 (2019).

APPENDIX A

Kendrick Mass Defect (KMD) Plots for Meteorites

In a KMD plot, carbon distribution and alkylation are easily viewable. Horizontal lines that can be drawn through data points represent homologous series of compounds with increasing alkylation belonging to the same heteroatom class (i.e. C_xH_yN with a DBE of 1 would be present in a horizontal line). The plots correspond to ESI (+) data for all meteorites analyzed, where each dot represents a specific compound identified. Figure captions include meteorite name, aqueous alteration scale value (if known), and total number of organics identified.

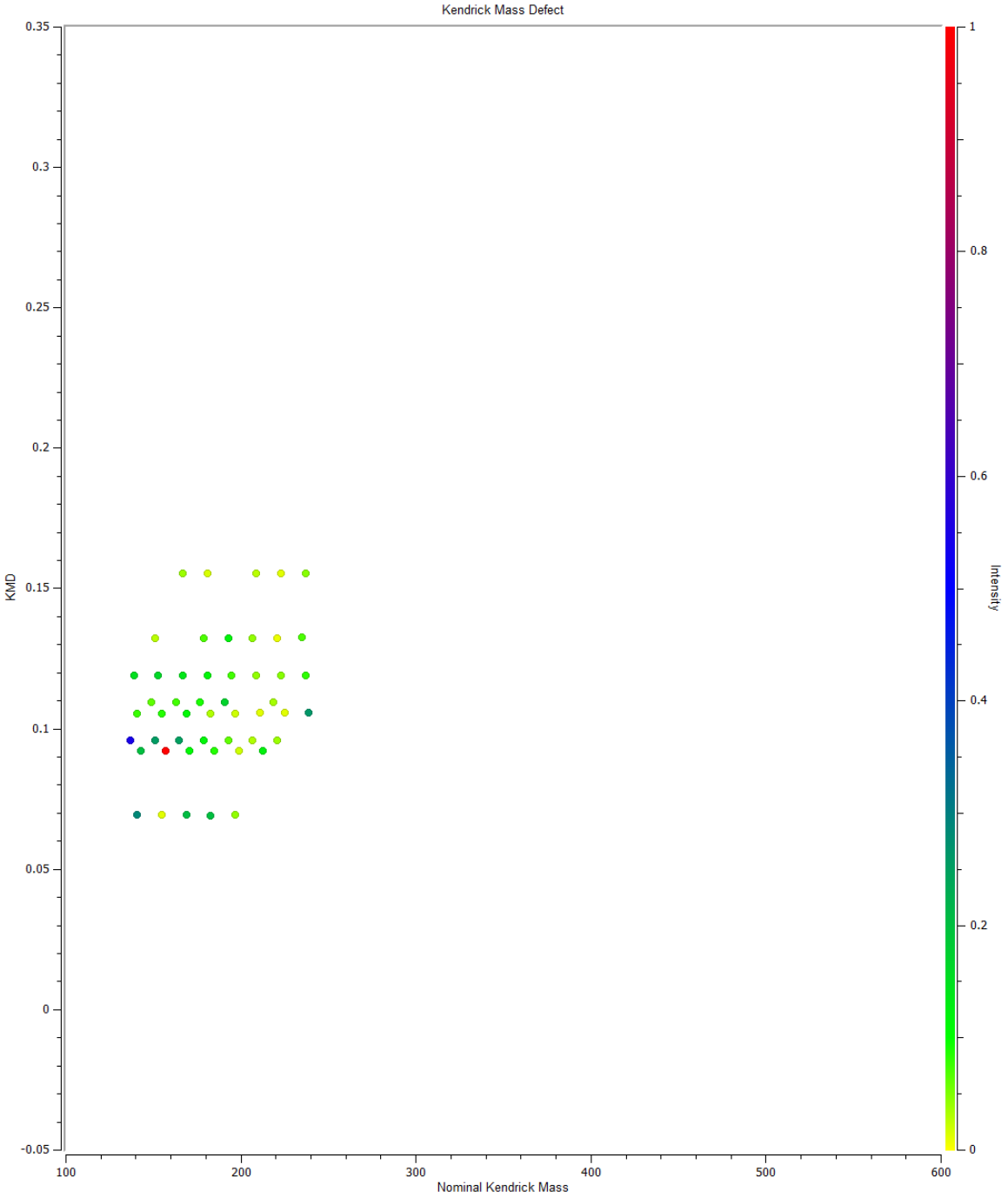

Figure 8: KMD Plot for EET 83355. Aqueous alteration value of 2.4 with 50 molecular formulas identified.

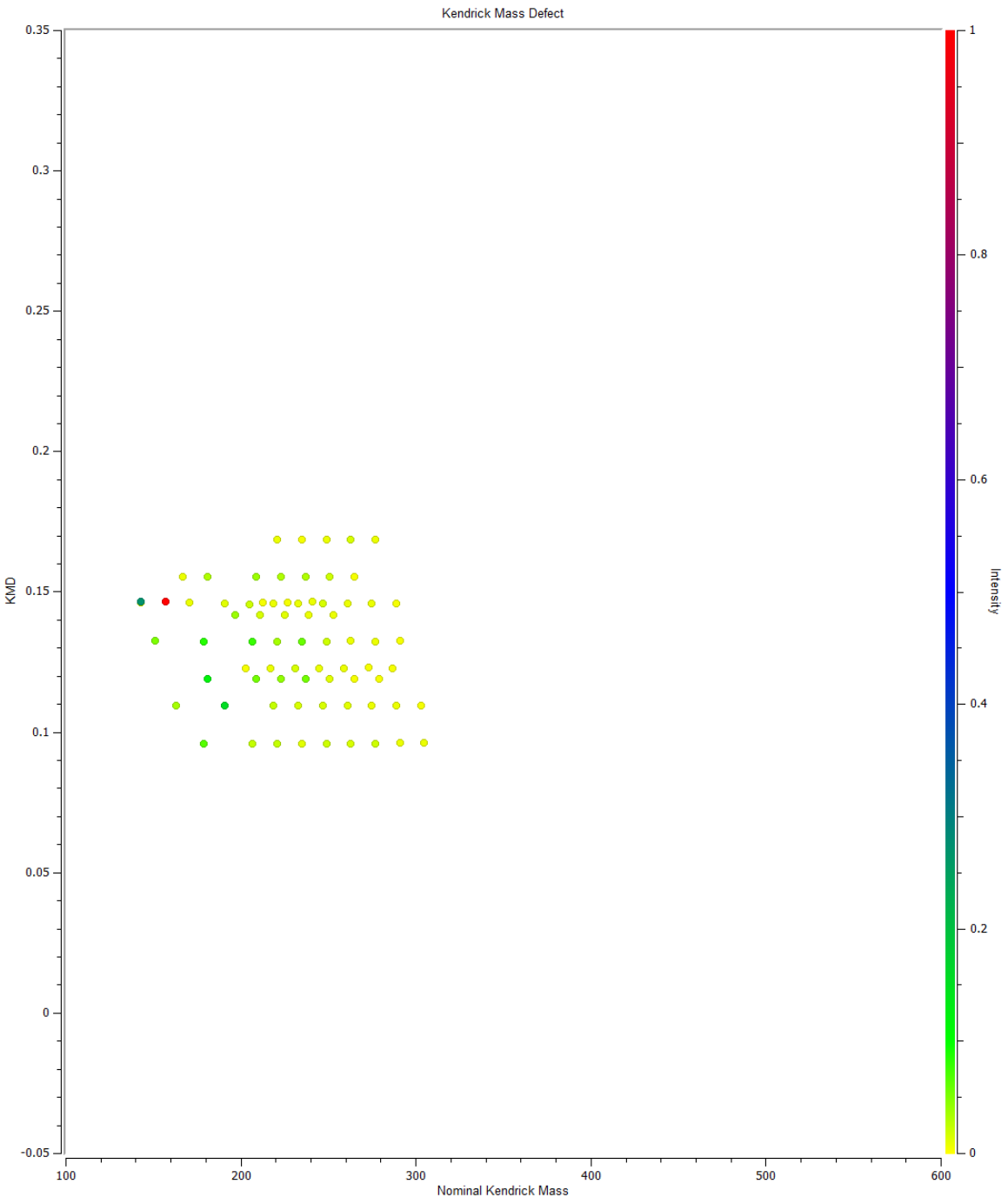

Figure 9: KMD Plot for MIL 07700. Aqueous alteration value of 2.2 with 72 molecular formulas identified.

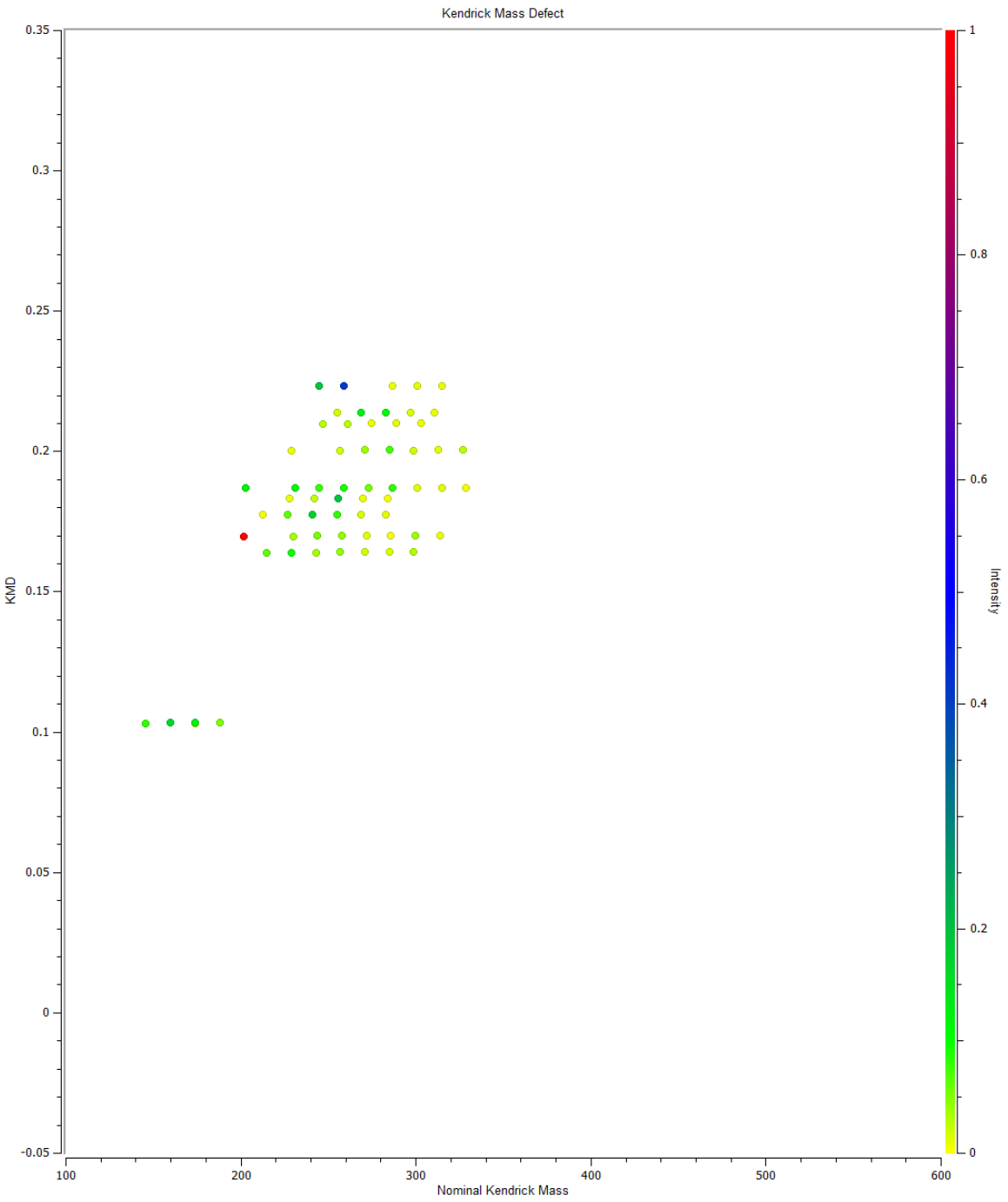

Figure 10: KMD Plot for ALH 84033. Aqueous alteration value of 2.1 with 61 molecular formulas identified.

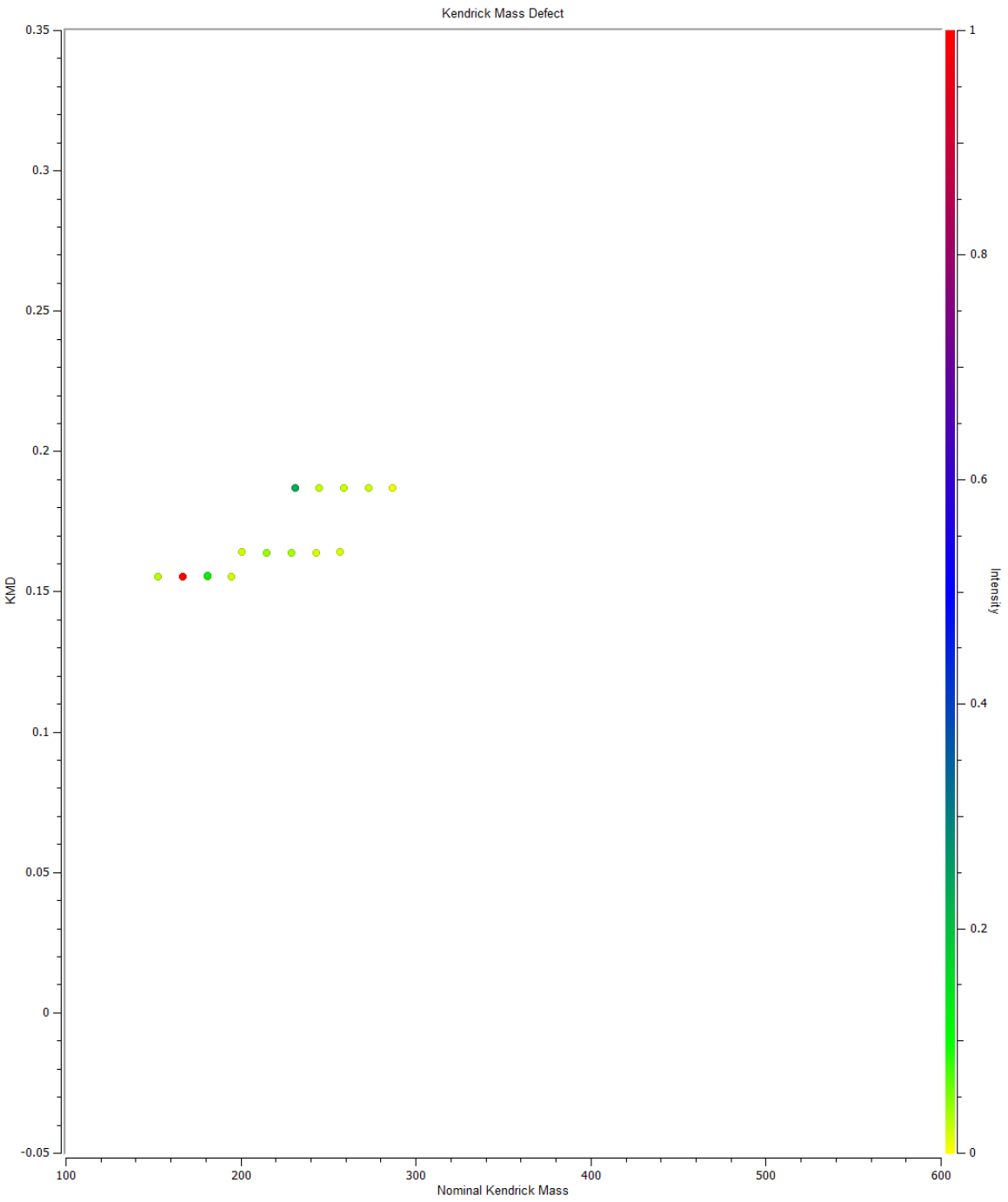

Figure 11: KMD Plot for EET 87522. Aqueous alteration value of 2.0 with 14 molecular formulas identified.

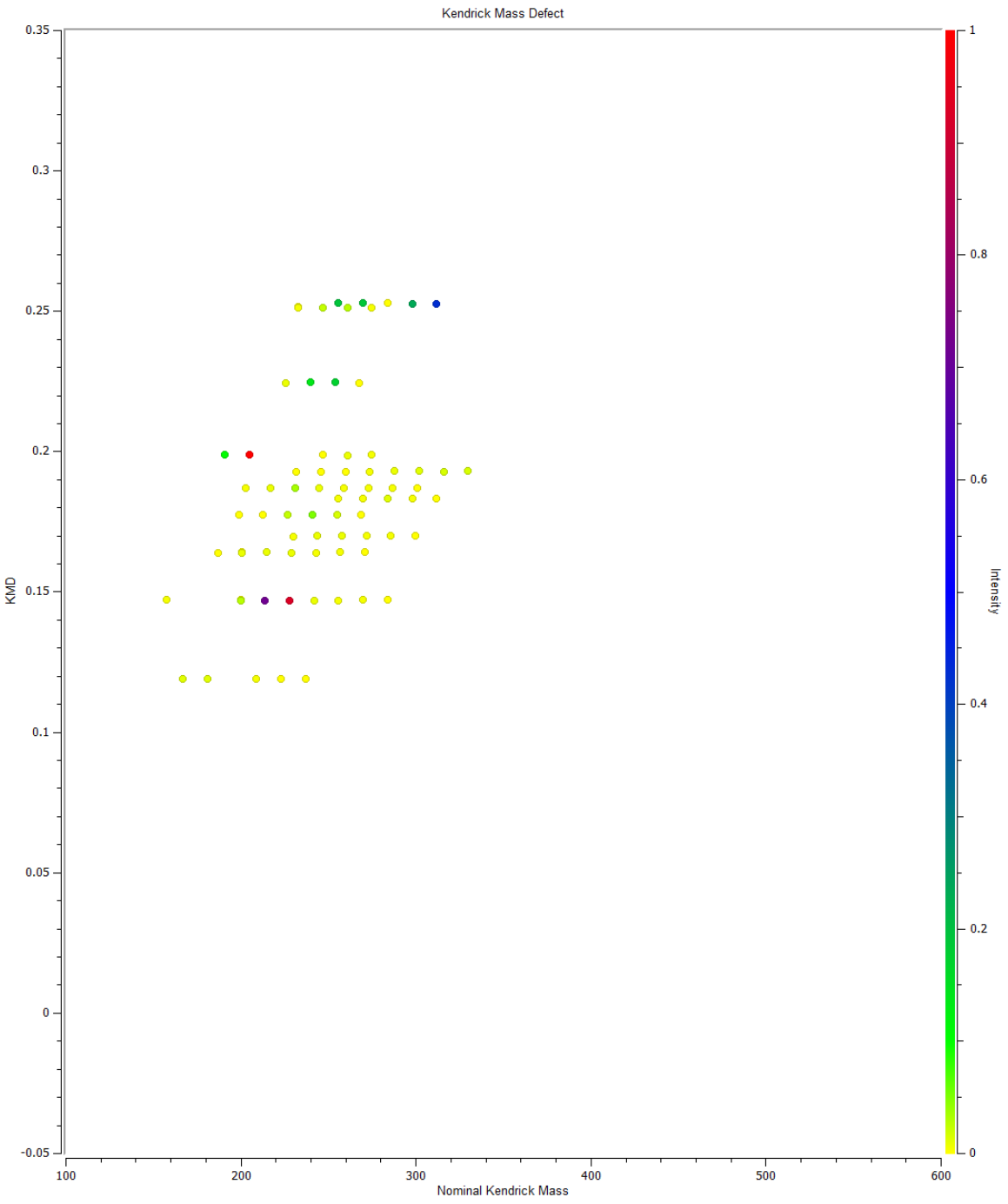

Figure 12: KMD Plot for PCA 91008. Aqueous alteration value of 2.0 with 71 molecular formulas identified.

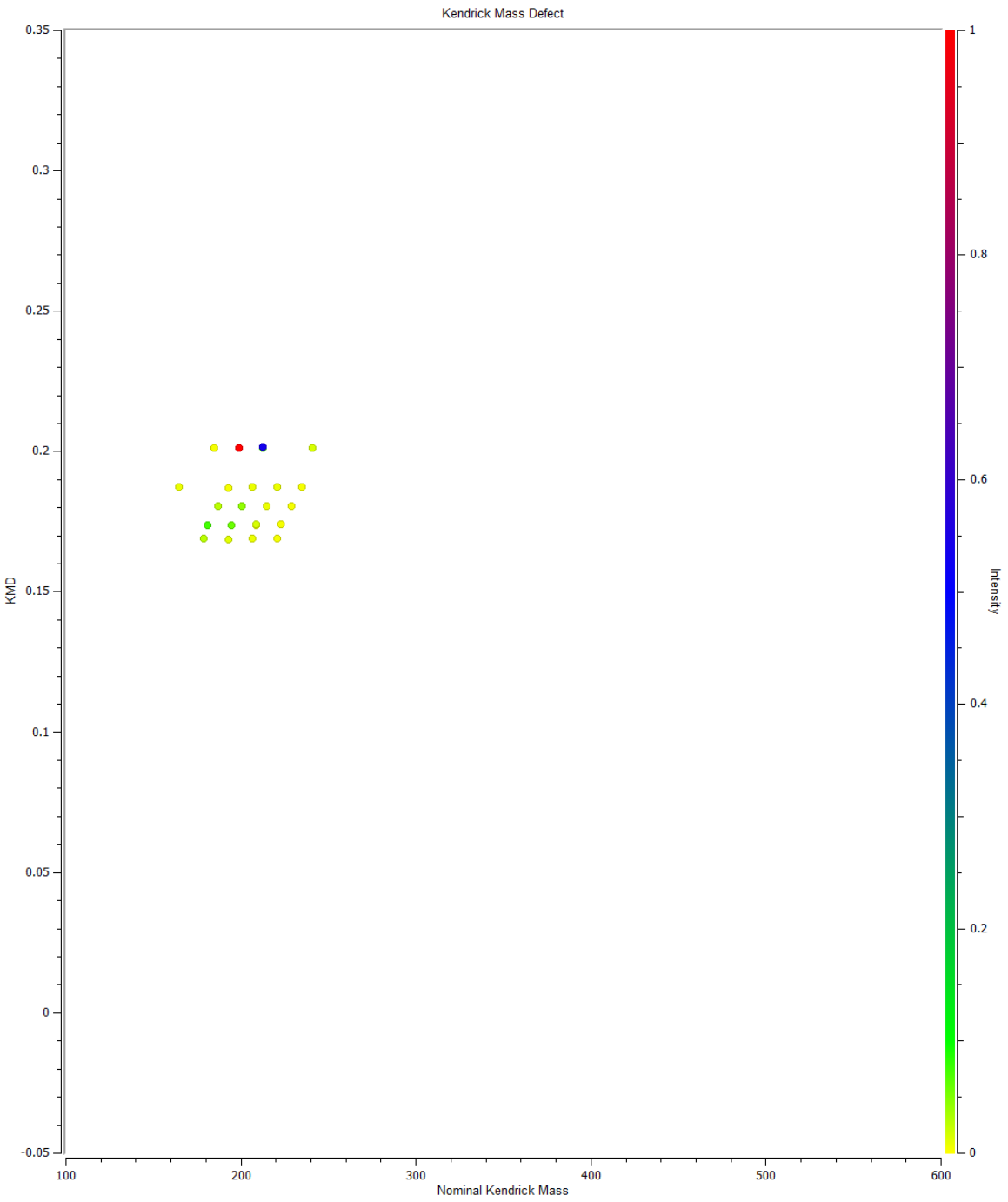

Figure 13: KMD Plot for EET 96029. Aqueous alteration value of 1.9 with 21 molecular formulas identified.

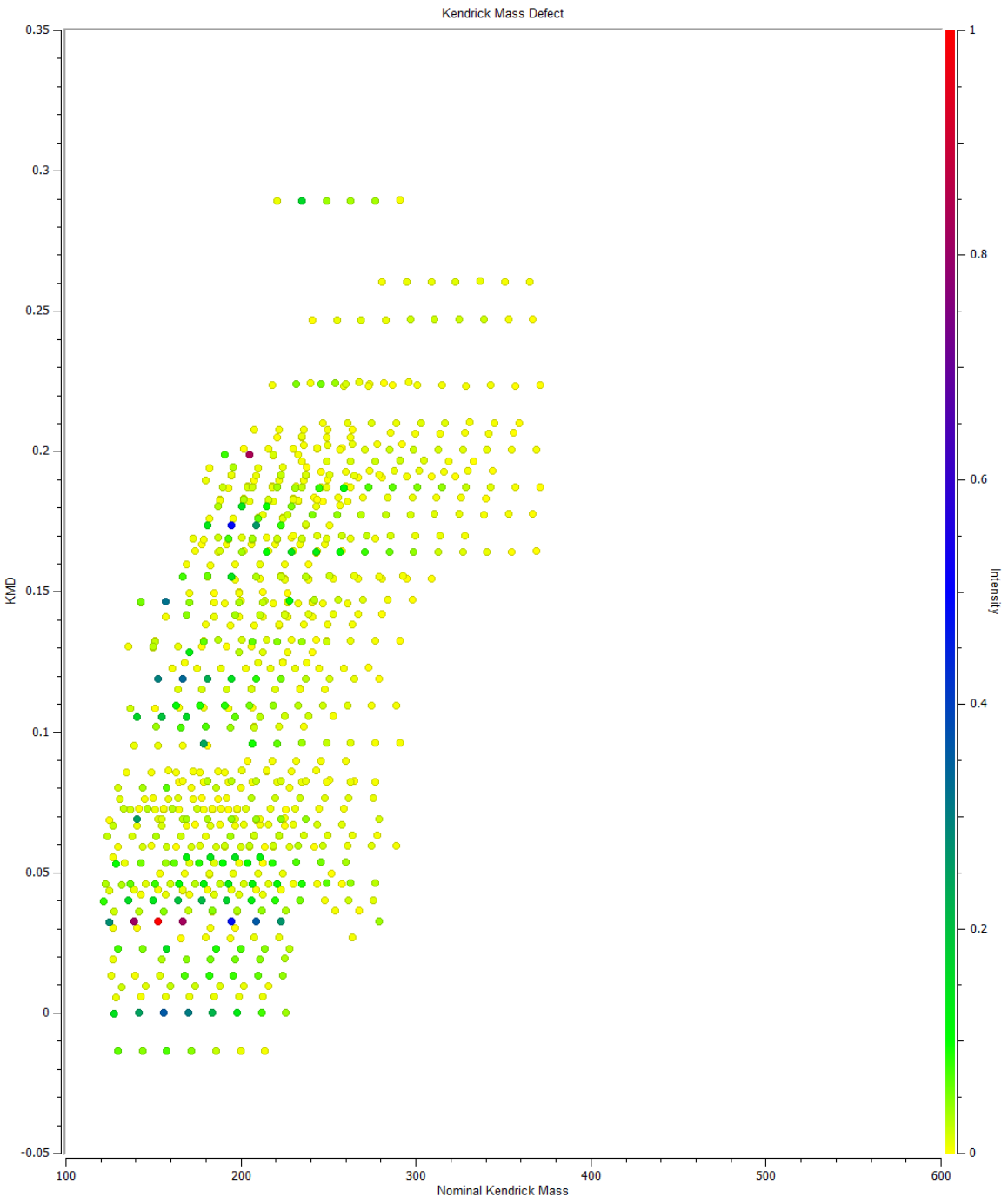

Figure 14: KMD Plot for LEW 85311. Aqueous alteration value of 1.9 with 712 molecular formulas identified.

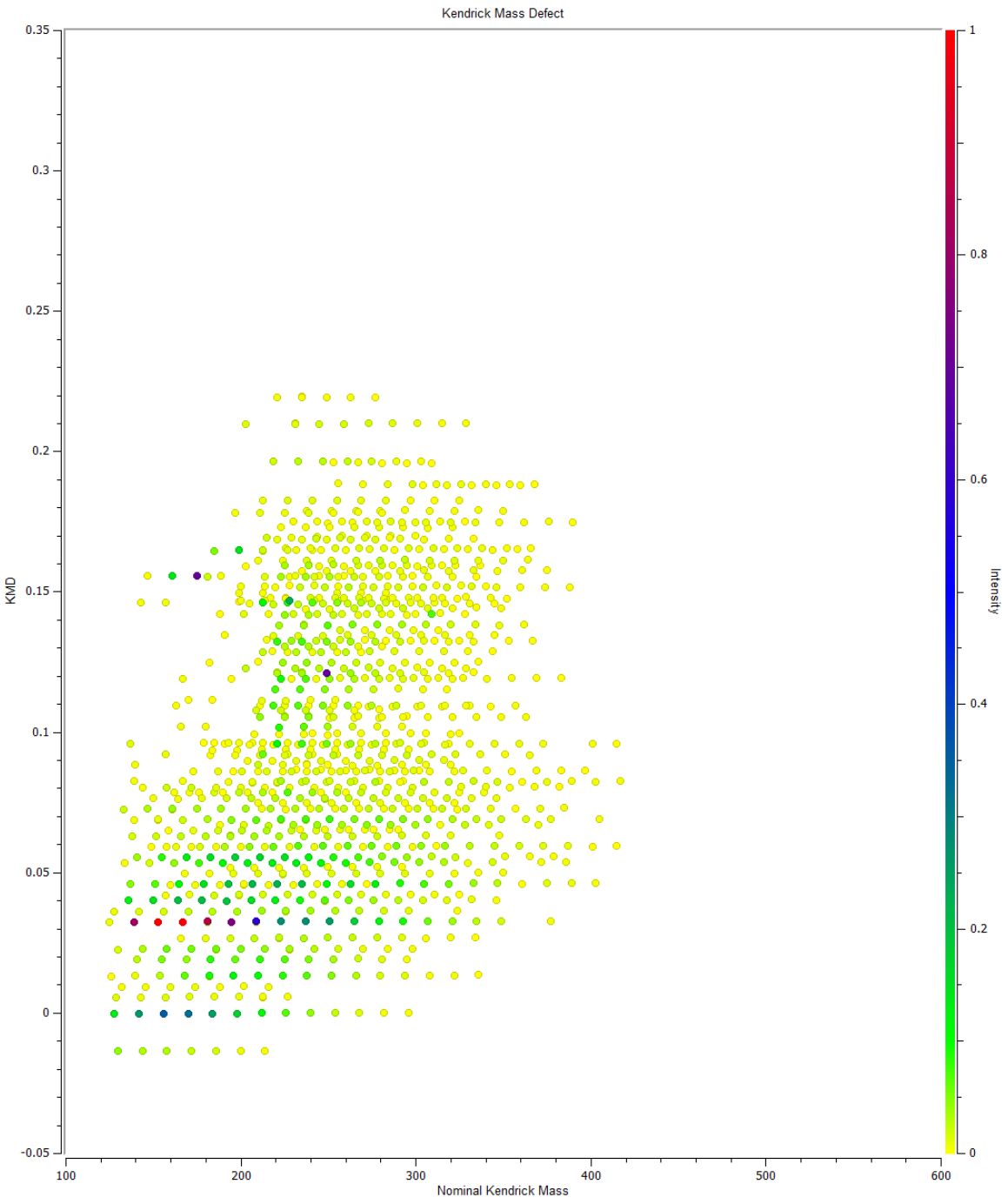

Figure 15: KMD Plot for TIL 91722. Aqueous alteration value of 1.9 with 1138 molecular formulas identified.

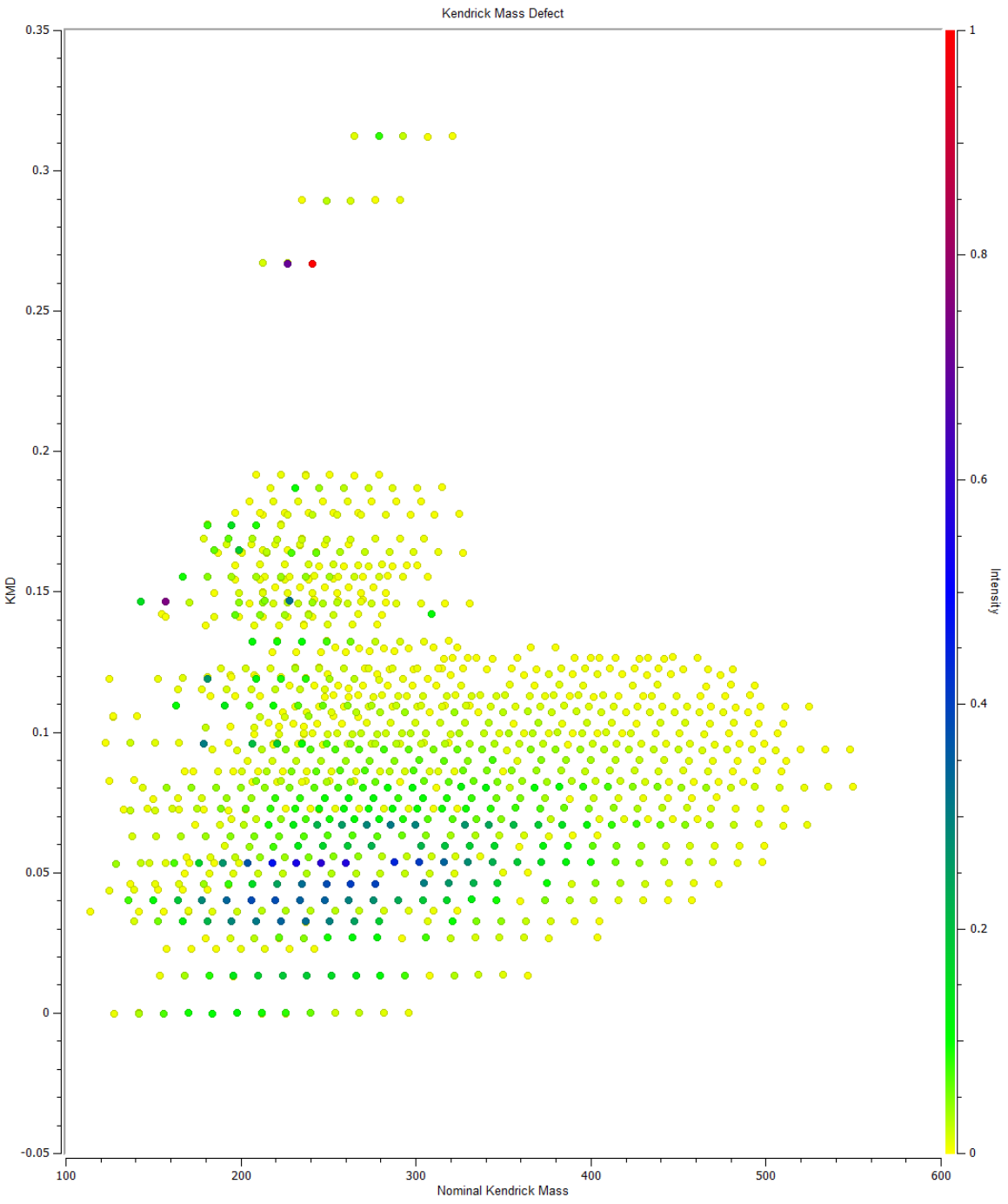

Figure 16: KMD Plot for LON 94101. Aqueous alteration value of 1.8 with 980 molecular formulas identified.

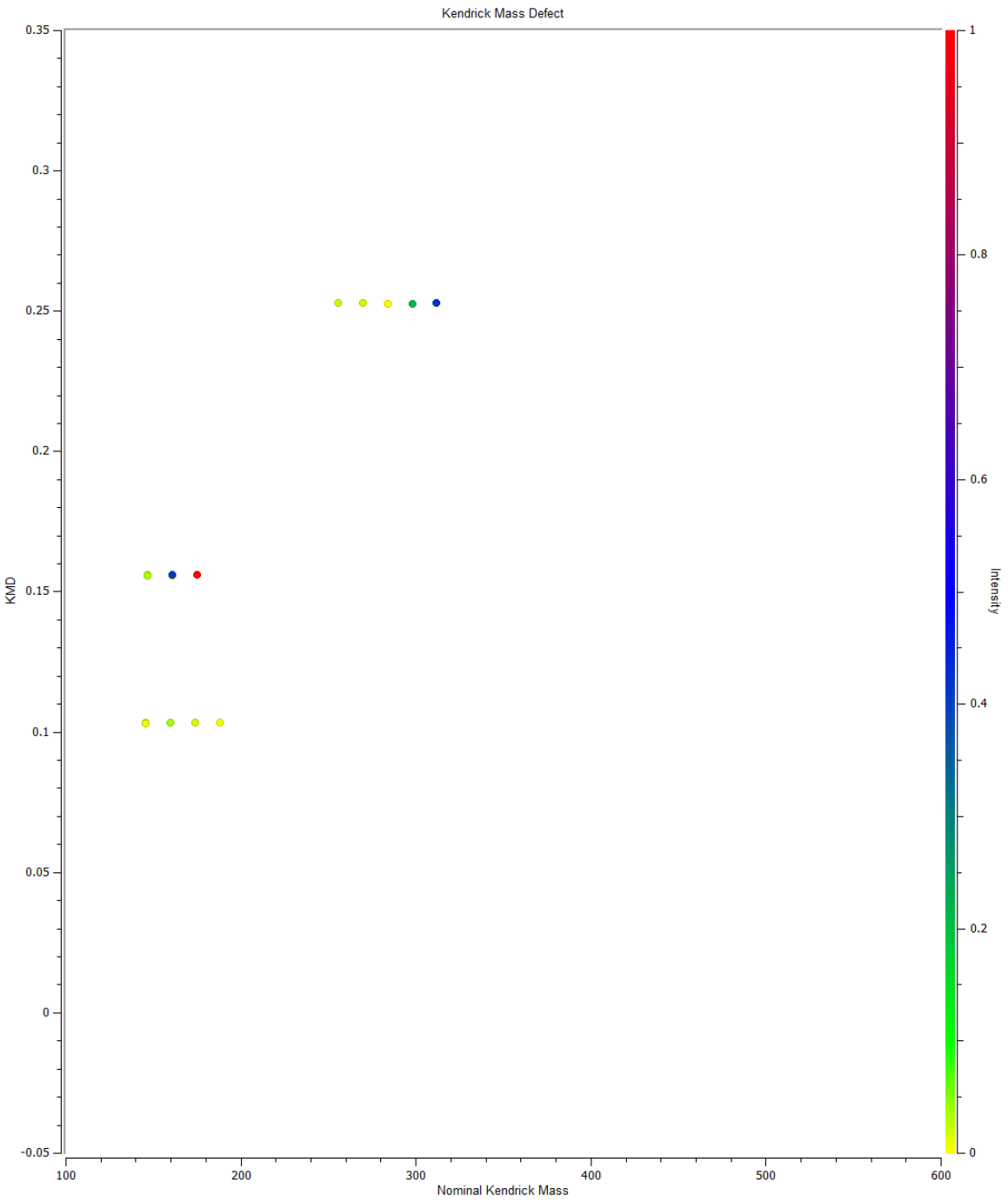

Figure 17: KMD Plot for MAC 88100. Aqueous alteration value of 1.7 with 12 molecular formulas identified.

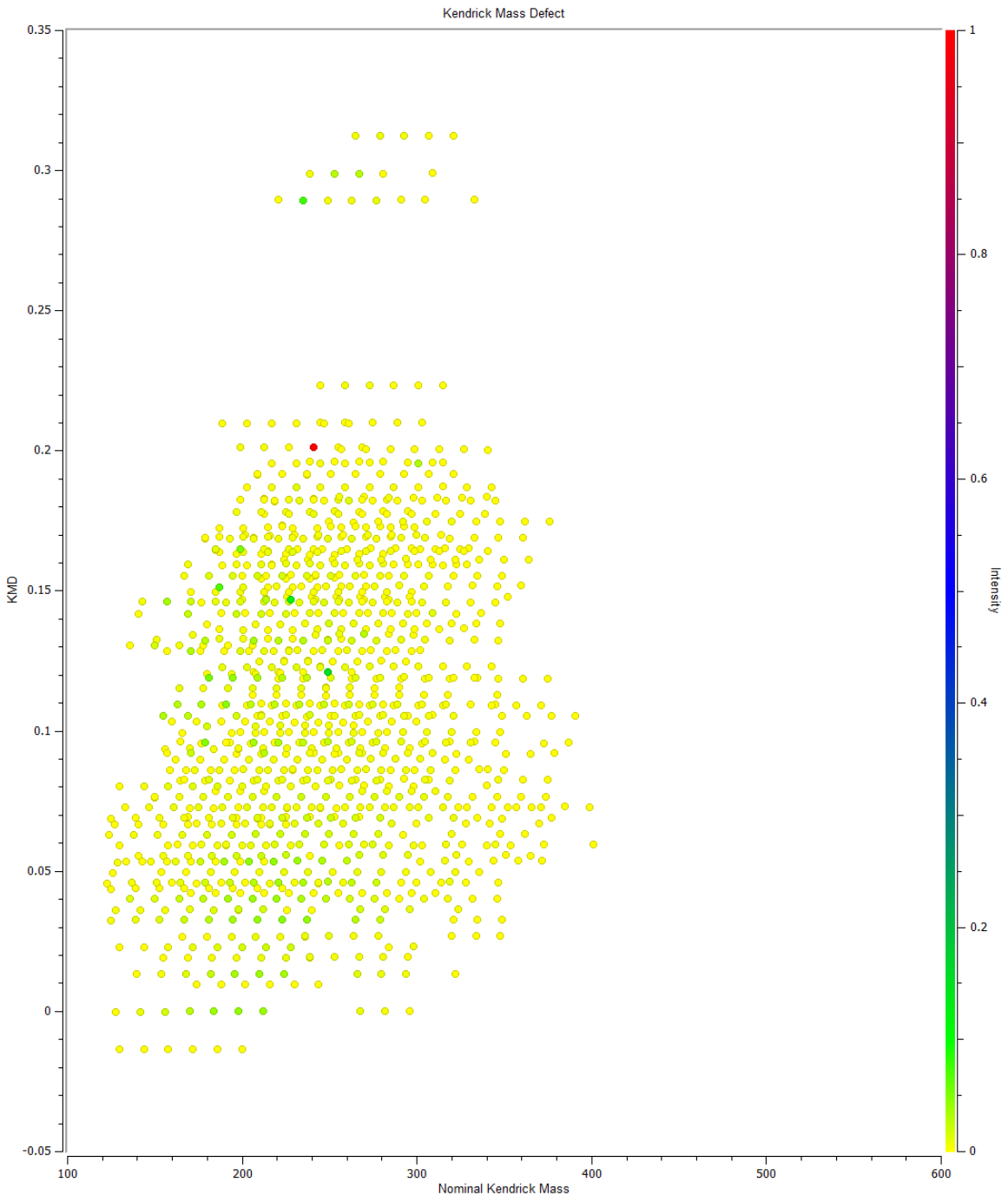

Figure 18: KMD Plot for QUE 97990. Aqueous alteration value of 1.7 with 1082 molecular formulas identified.

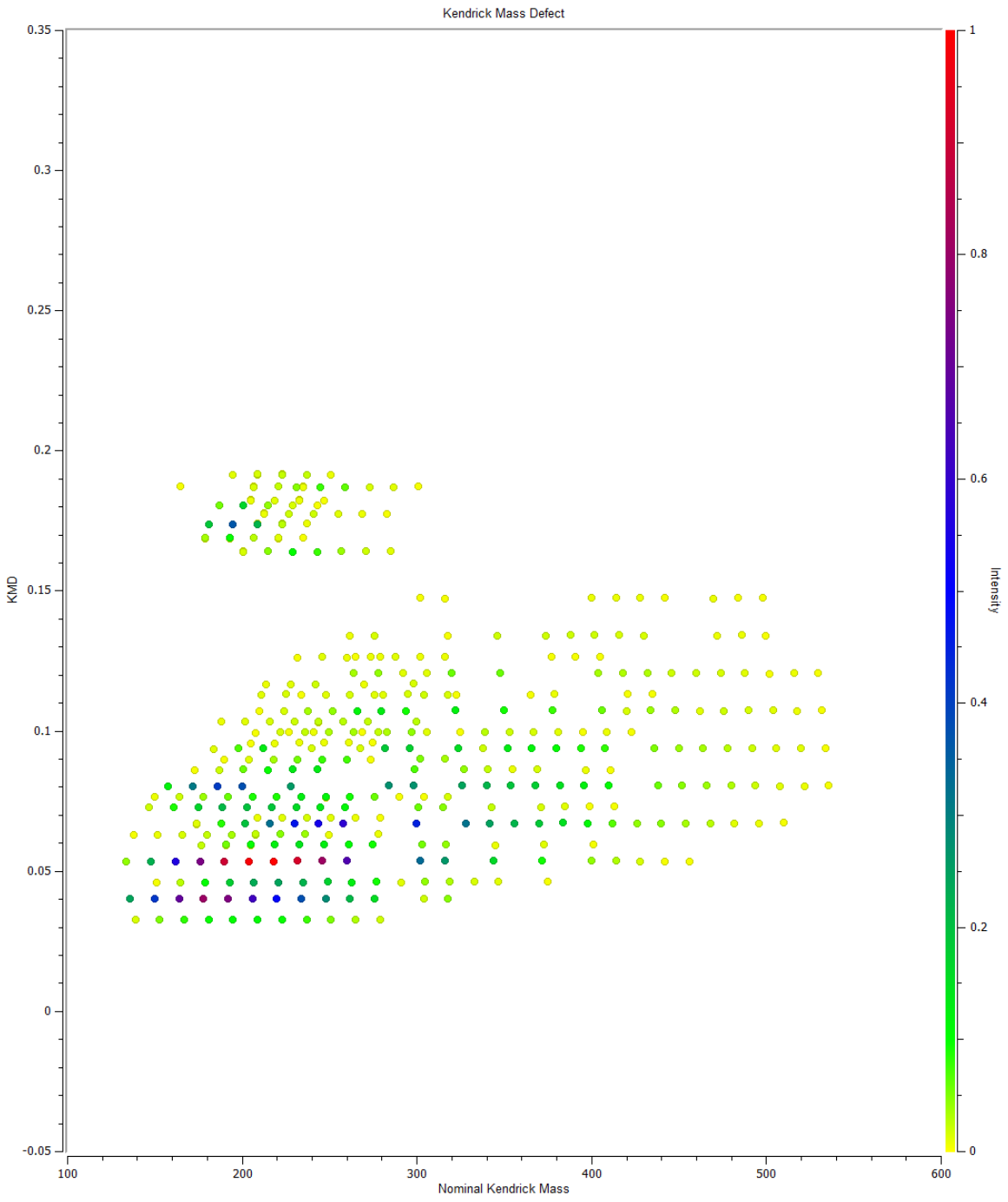

Figure 19: KMD Plot for DOM 03183. Aqueous alteration value of 1.6 with 375 molecular formulas identified.

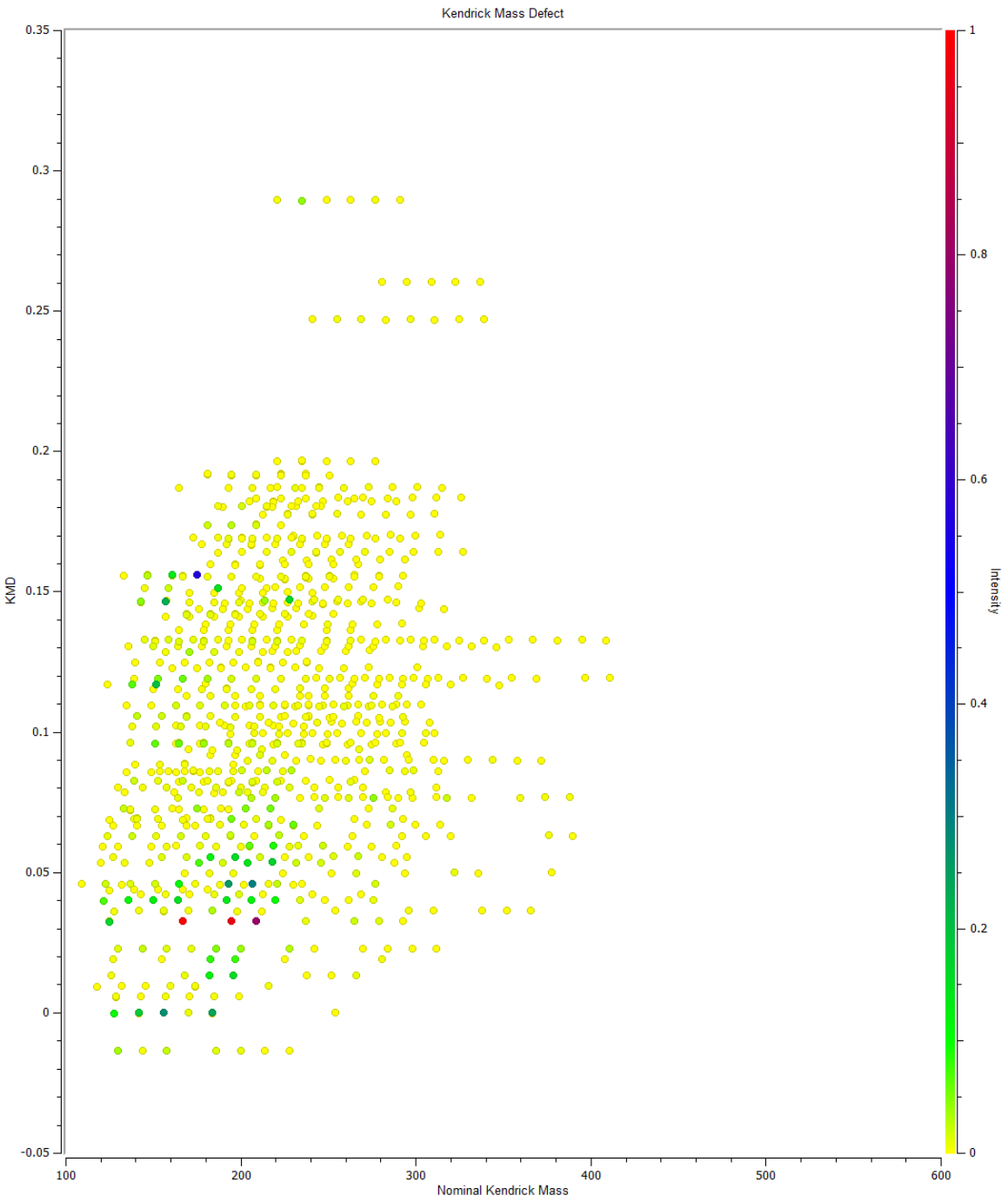

Figure 20: KMD Plot for GRO 95566. Aqueous alteration value of 1.6 with 805 molecular formulas identified.

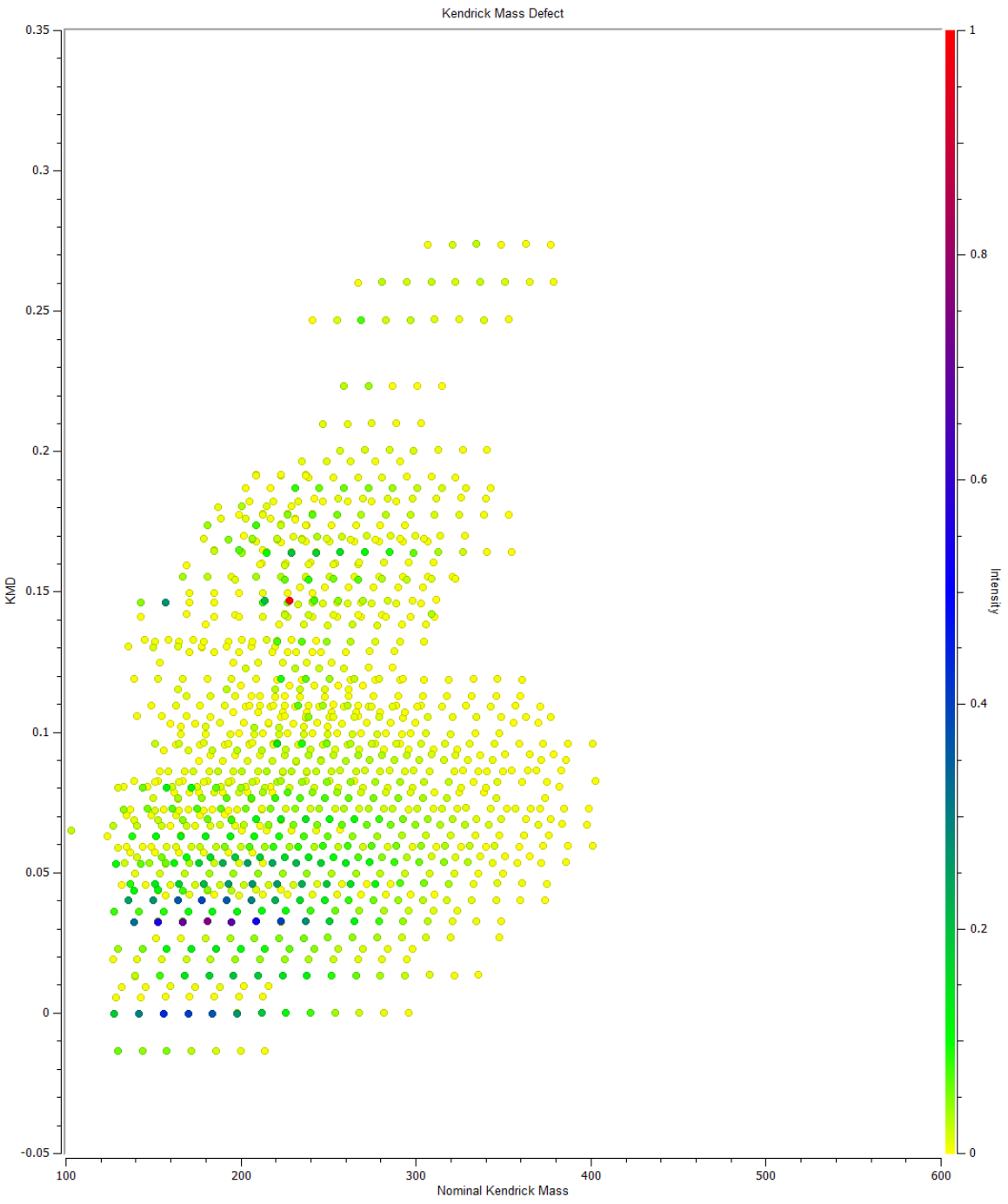

Figure 21: KMD Plot for LEW 88001. Aqueous alteration value of 1.6 with 1036 molecular formulas identified.

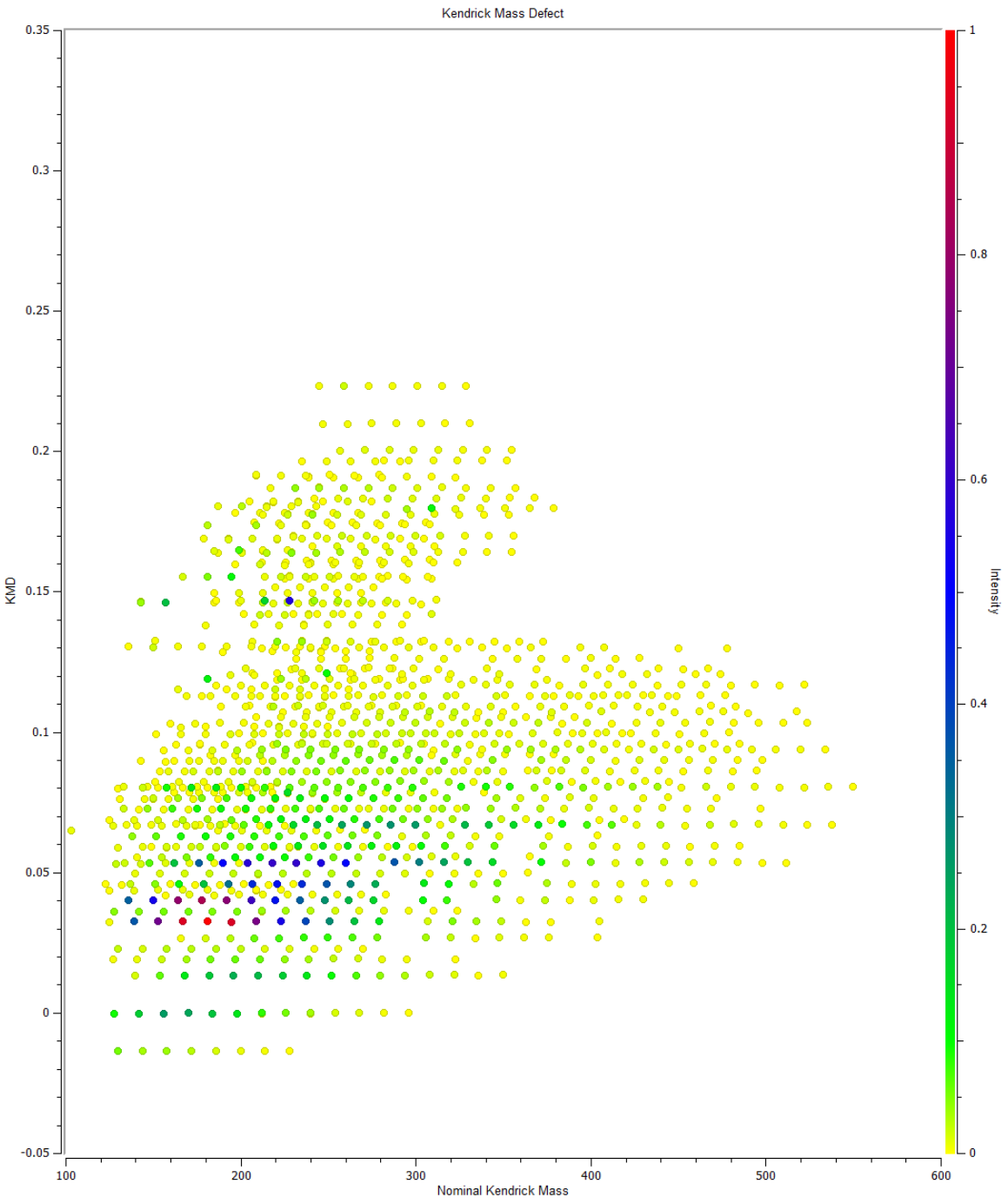

Figure 22: KMD Plot for LEW 90500. Aqueous alteration value of 1.6 with 1243 molecular formulas identified.

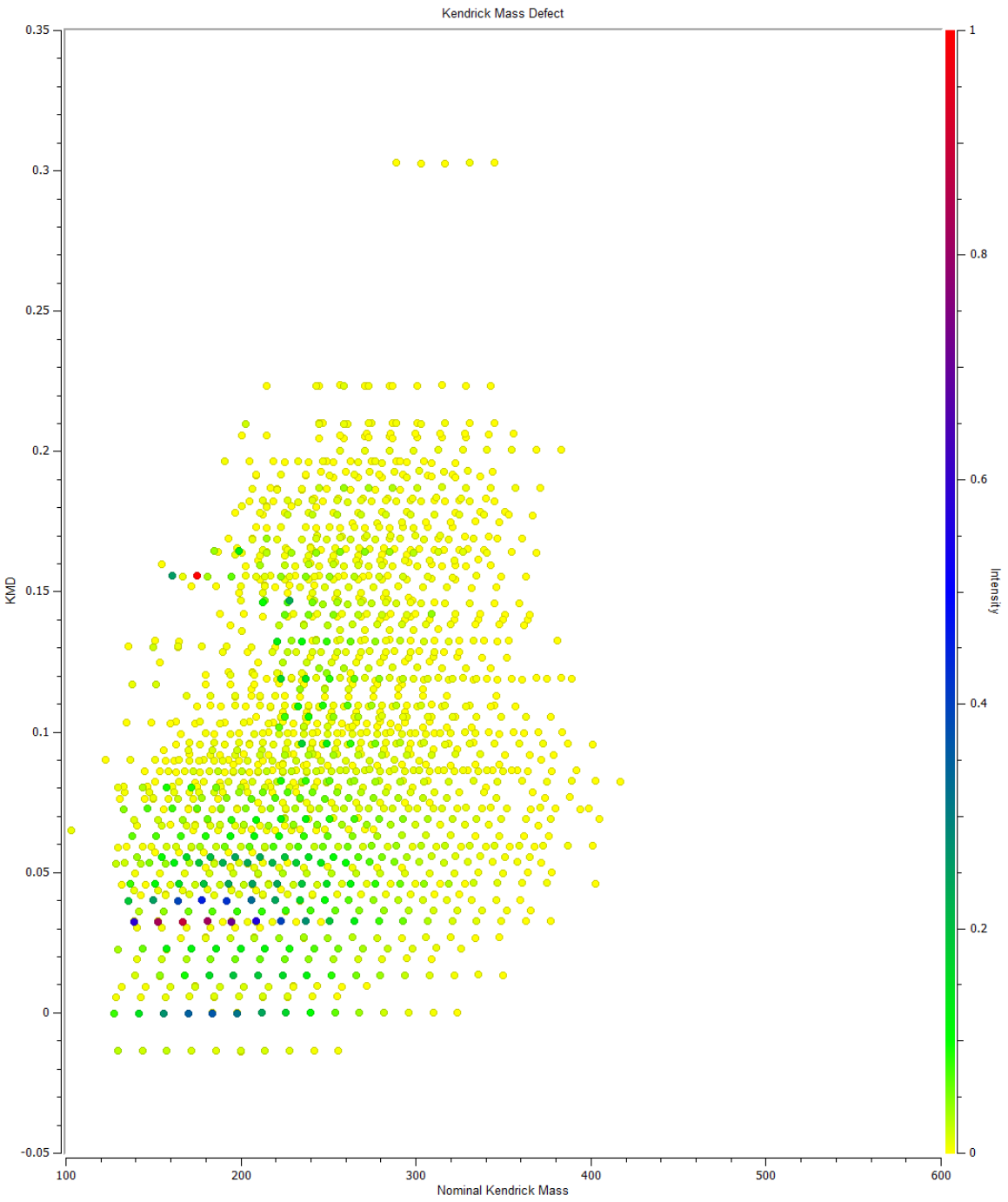

Figure 23: KMD Plot for LAP 02333. Aqueous alteration value of 1.5 with 1452 molecular formulas identified.

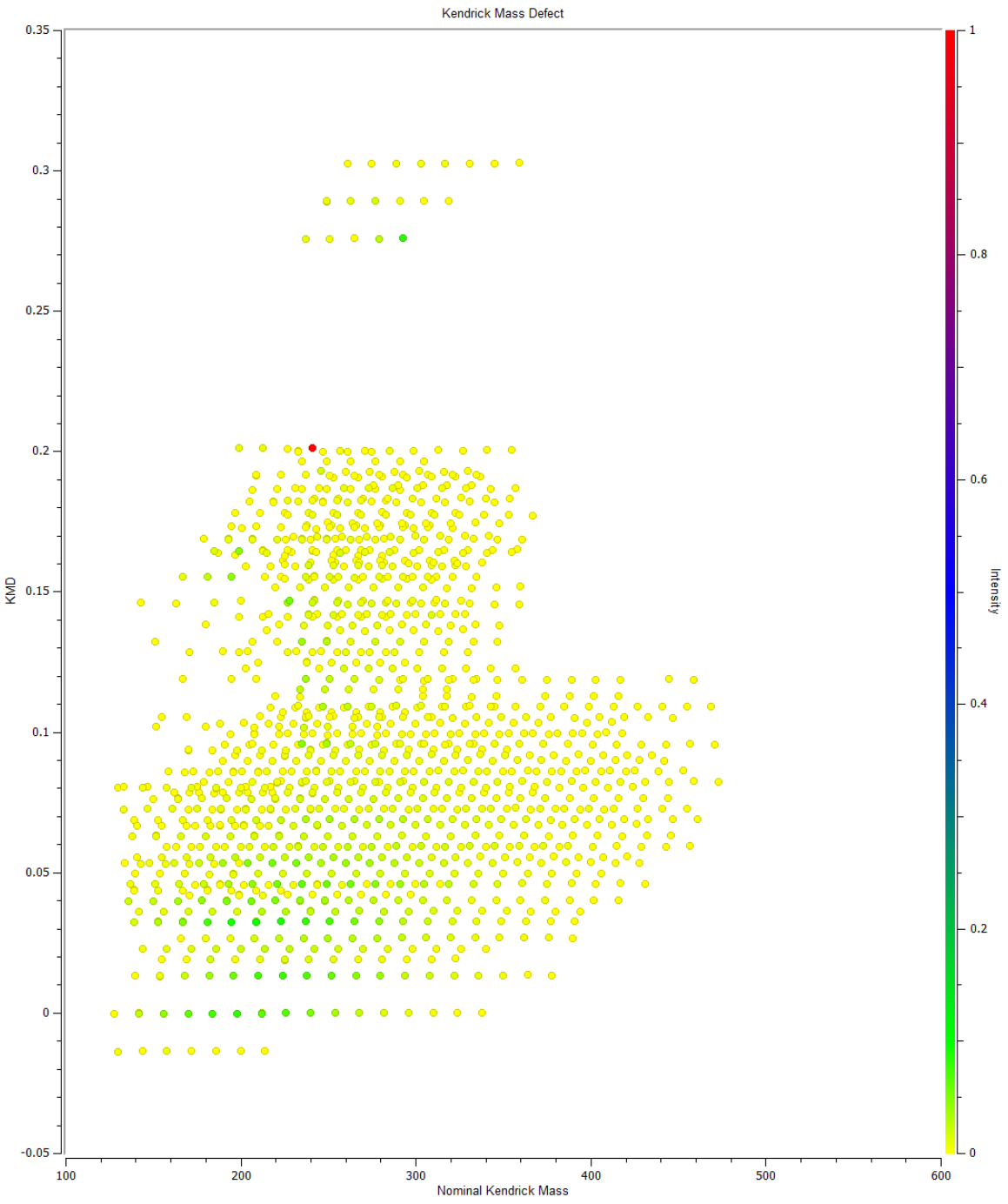

Figure 24: KMD Plot for ALH 85013. Aqueous alteration value of 1.4 with 1195 molecular formulas identified.

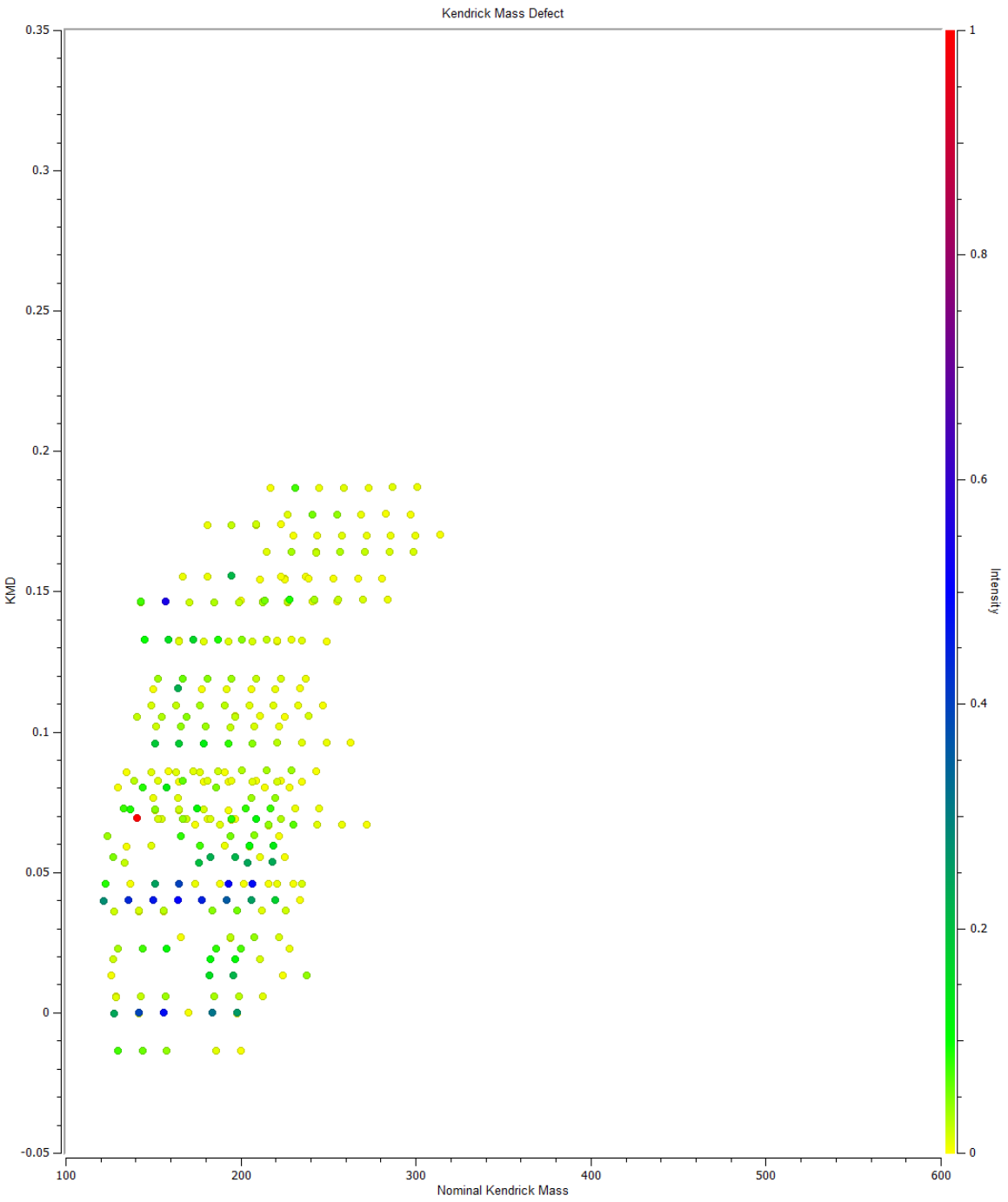

Figure 25: KMD Plot for EET 96016. Aqueous alteration value of 1.4 with 265 molecular formulas identified.

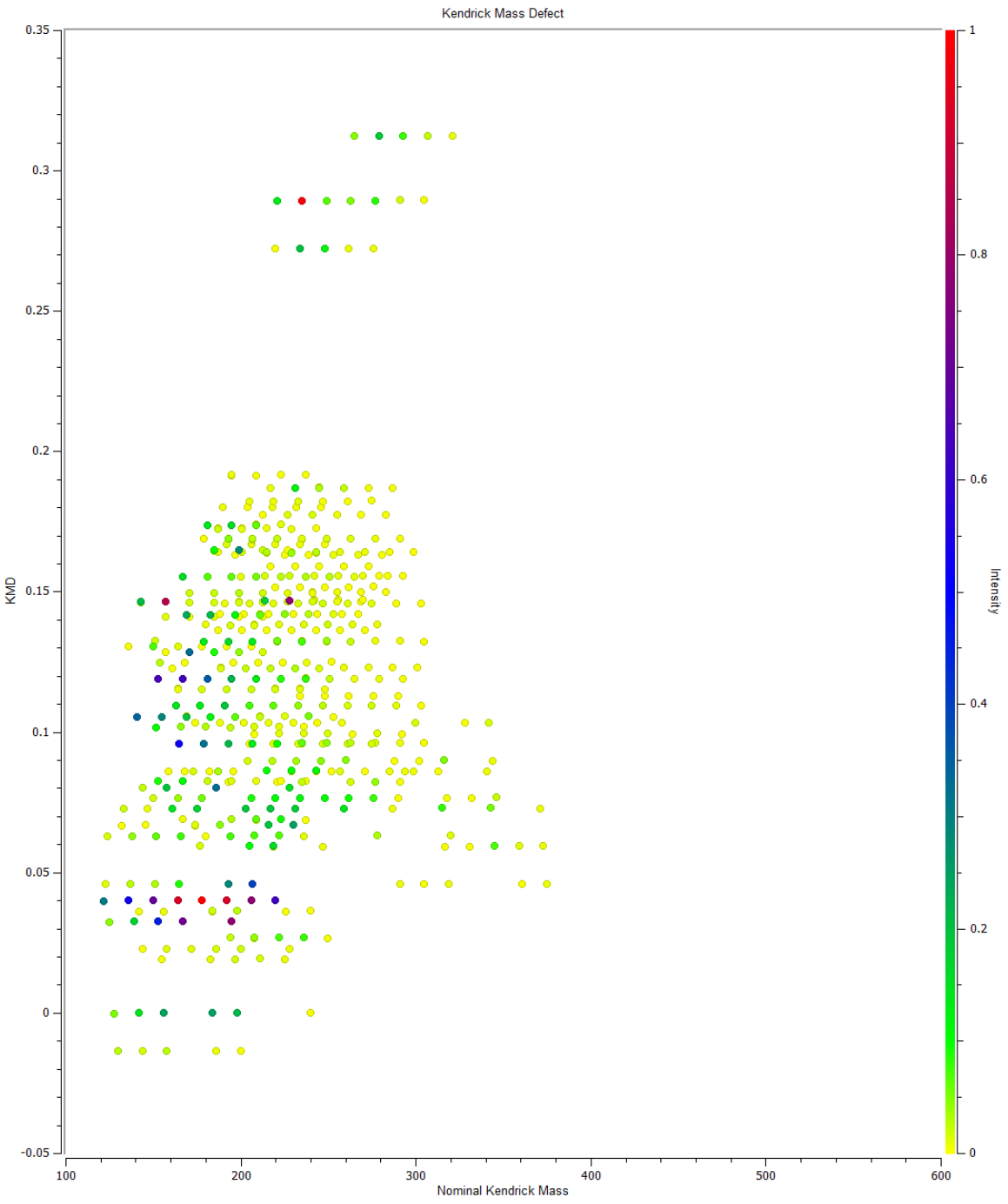

Figure 26: KMD Plot for LEW 87022. Aqueous alteration value of 1.4 with 459 molecular formulas identified.

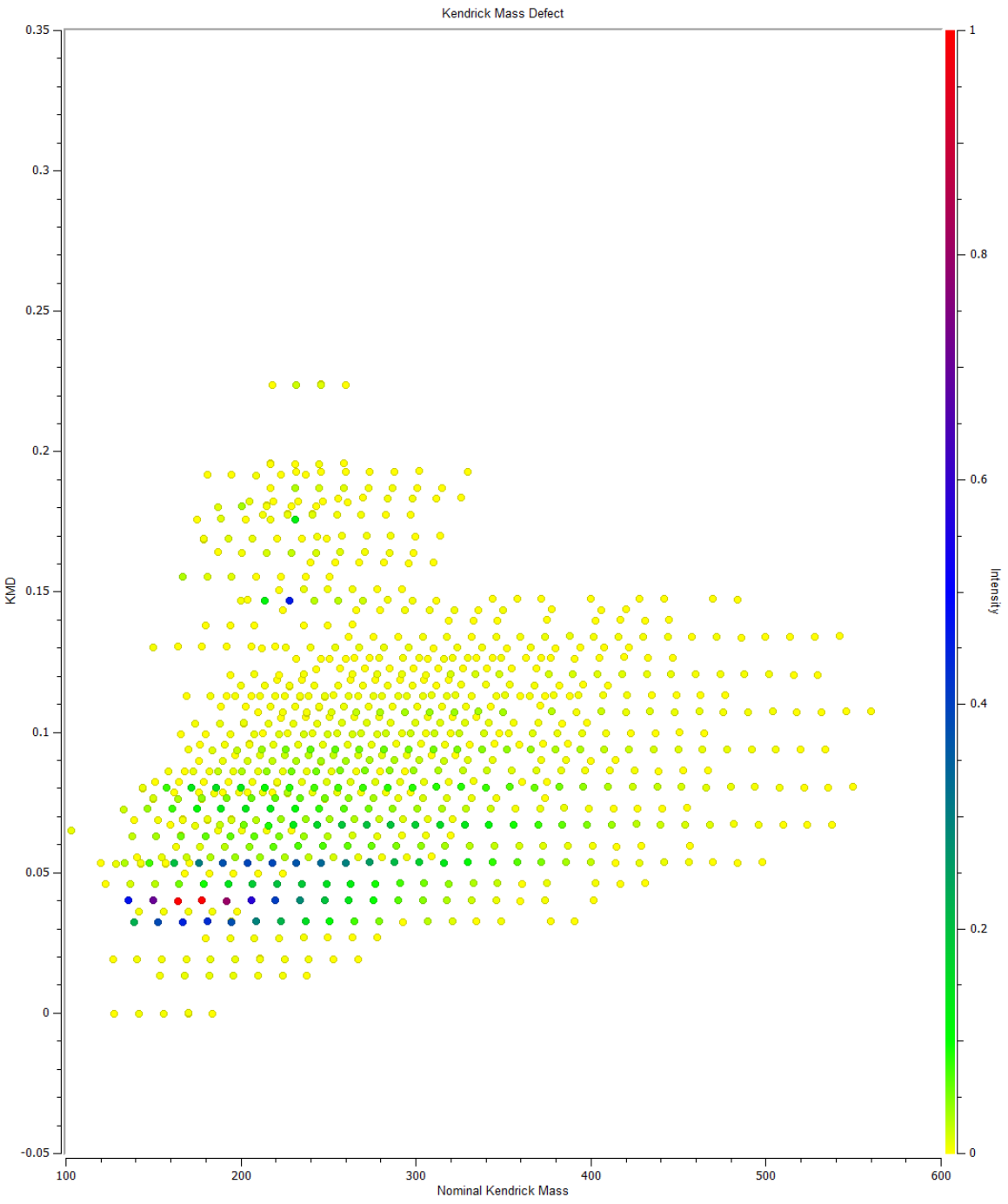

Figure 27: KMD Plot for MAC 88176. Aqueous alteration value of 1.4 with 824 molecular formulas identified.

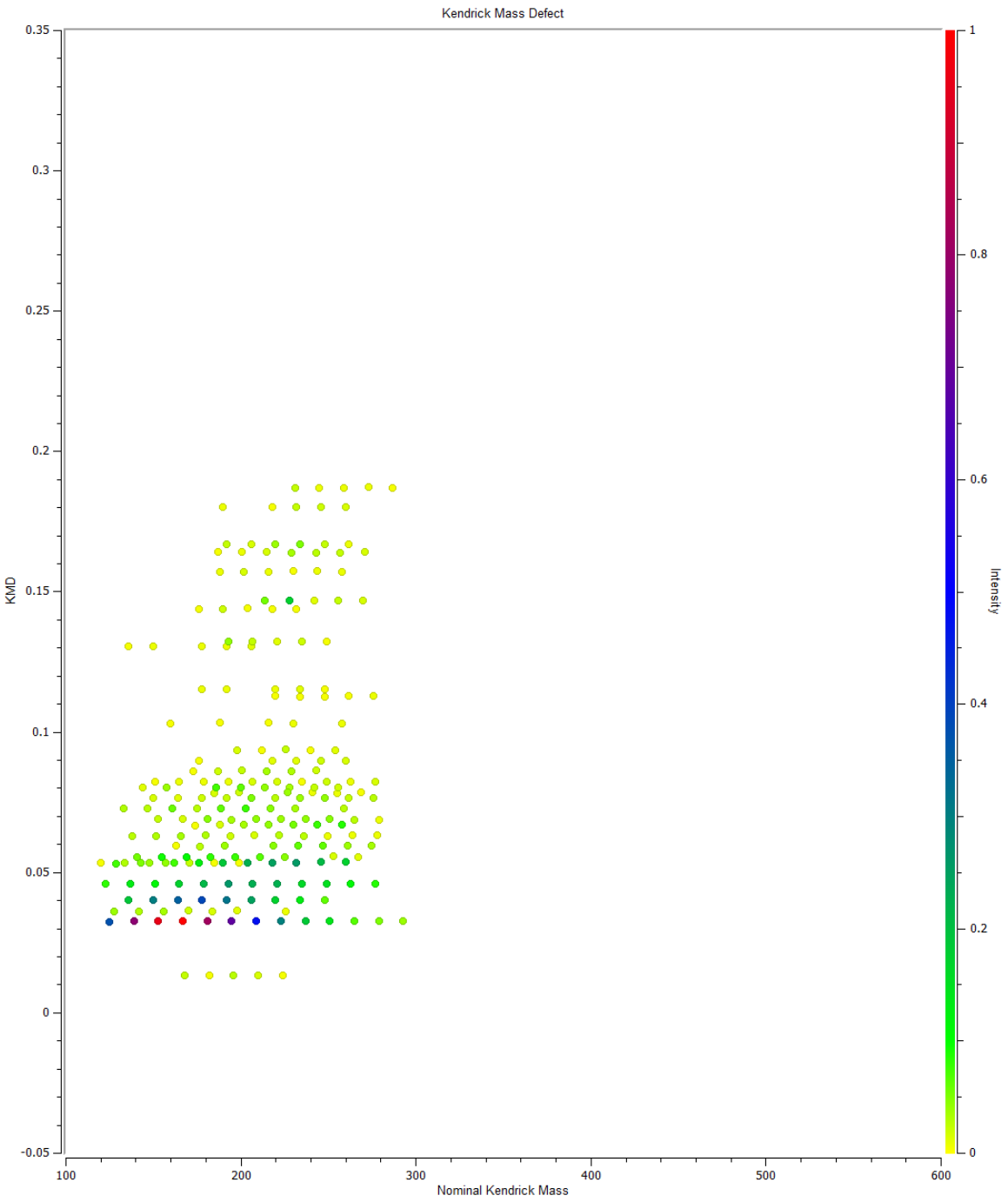

Figure 28: KMD Plot for LEW 87148. Aqueous alteration value of 1.3 with 231 molecular formulas identified.

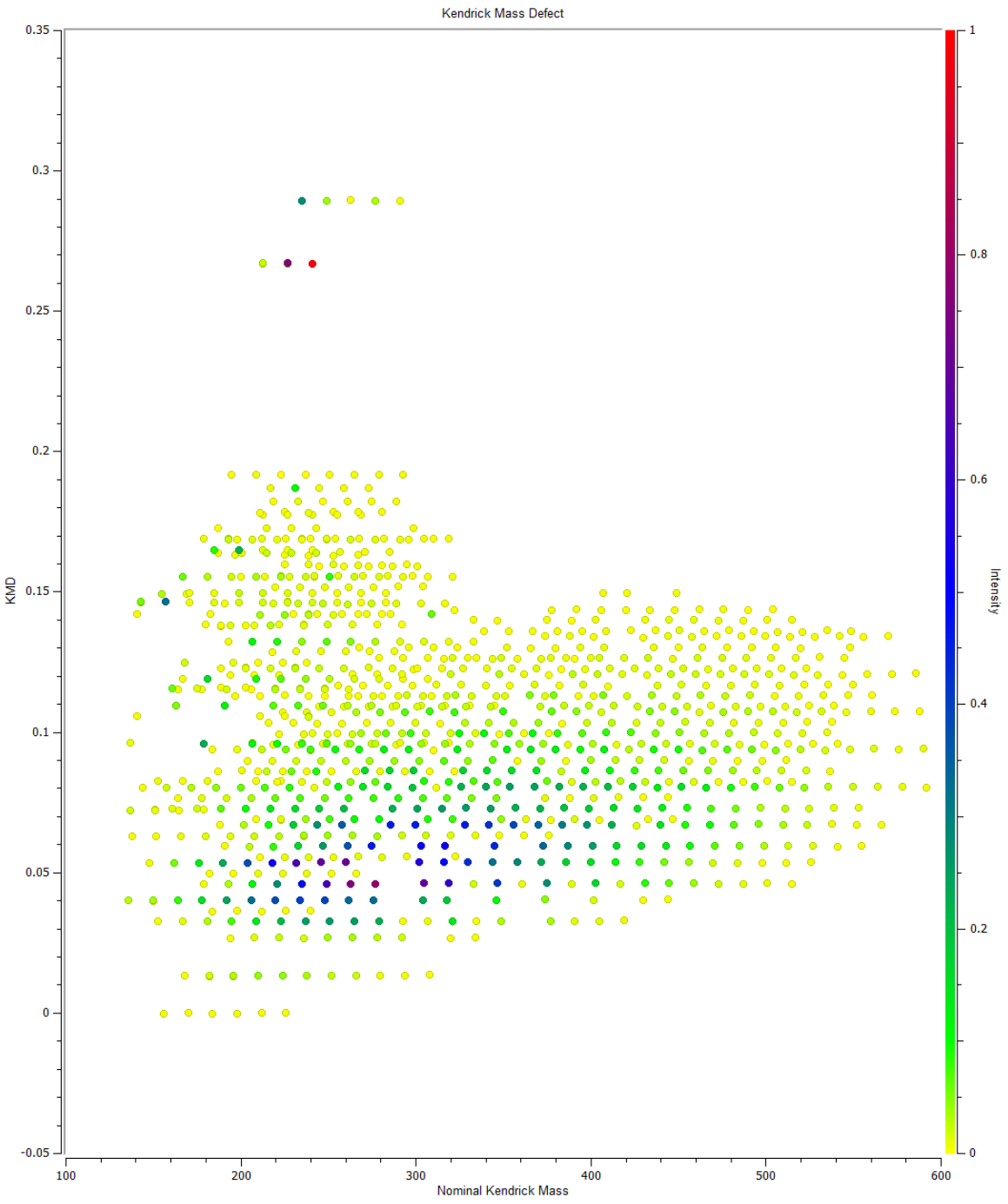

Figure 29: KMD Plot for ALH 84029. Aqueous alteration value of 1.2 with 991 molecular formulas identified.

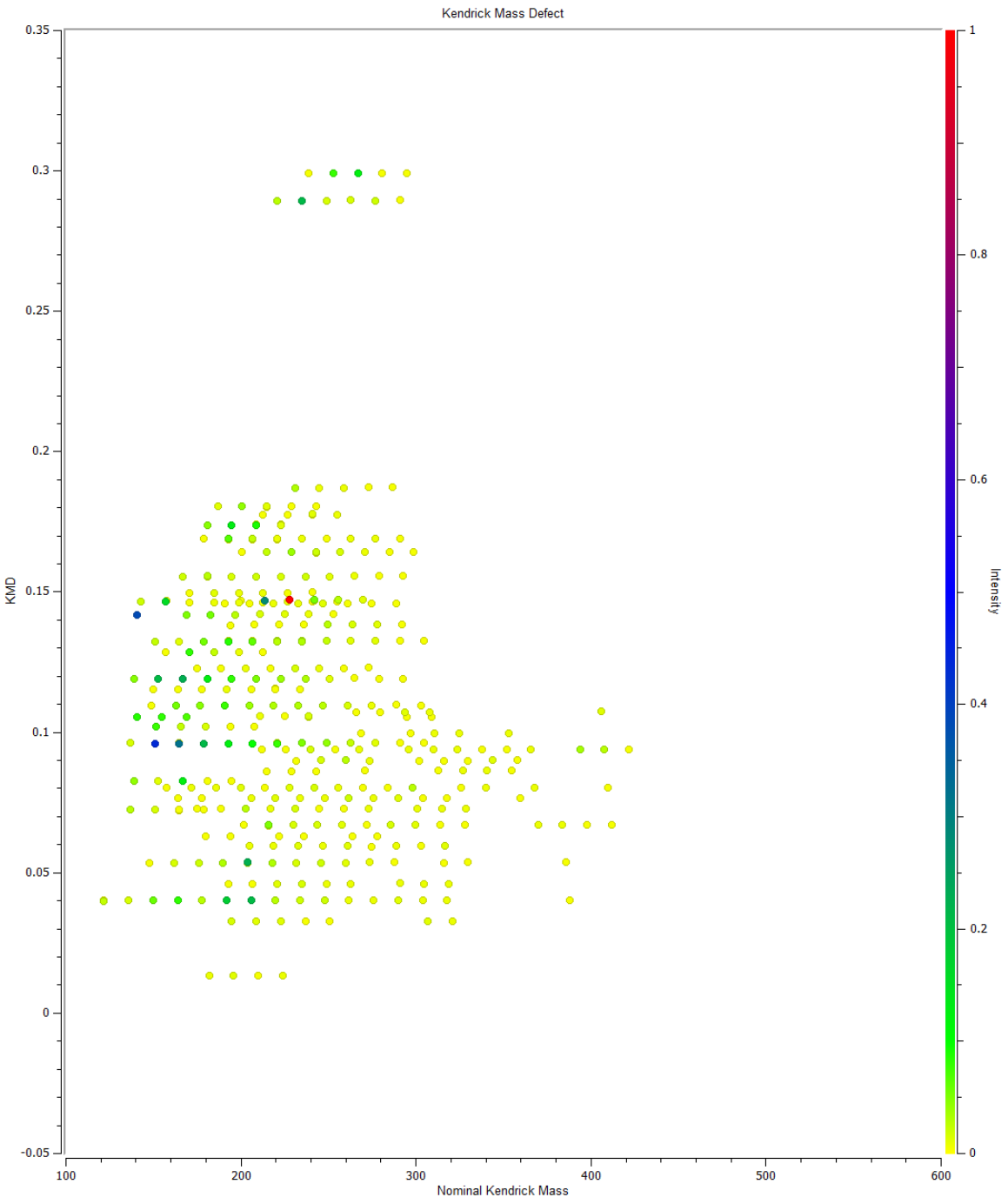

Figure 30: KMD Plot for ALH 84042. Aqueous alteration value of 1.2 with 351 molecular formulas identified.

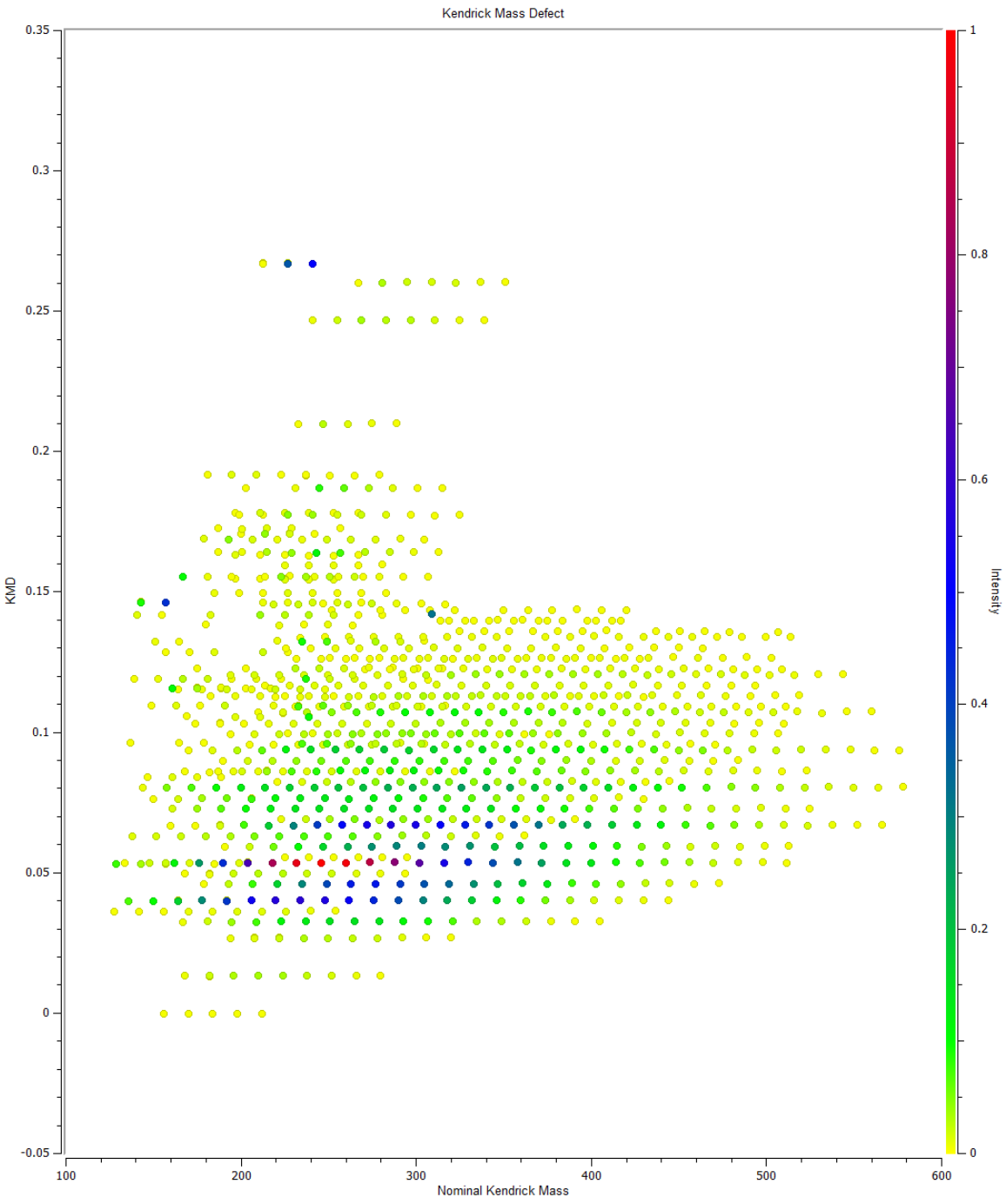

Figure 31: KMD Plot for ALH 84044. Aqueous alteration value of 1.2 with 989 molecular formulas identified.

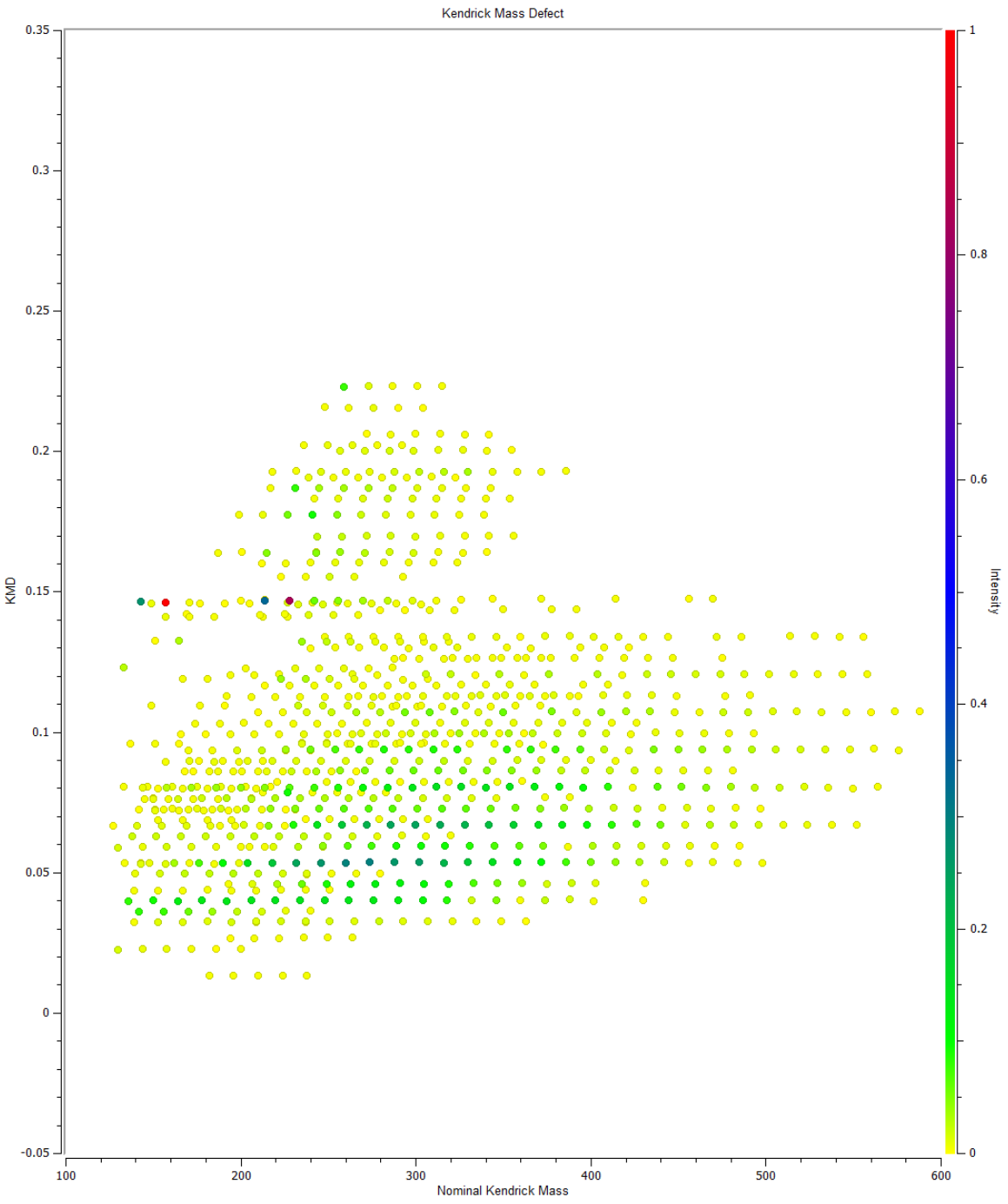

Figure 32: KMD Plot for MET 01070. Aqueous alteration value of 1.2 with 836 molecular formulas identified.

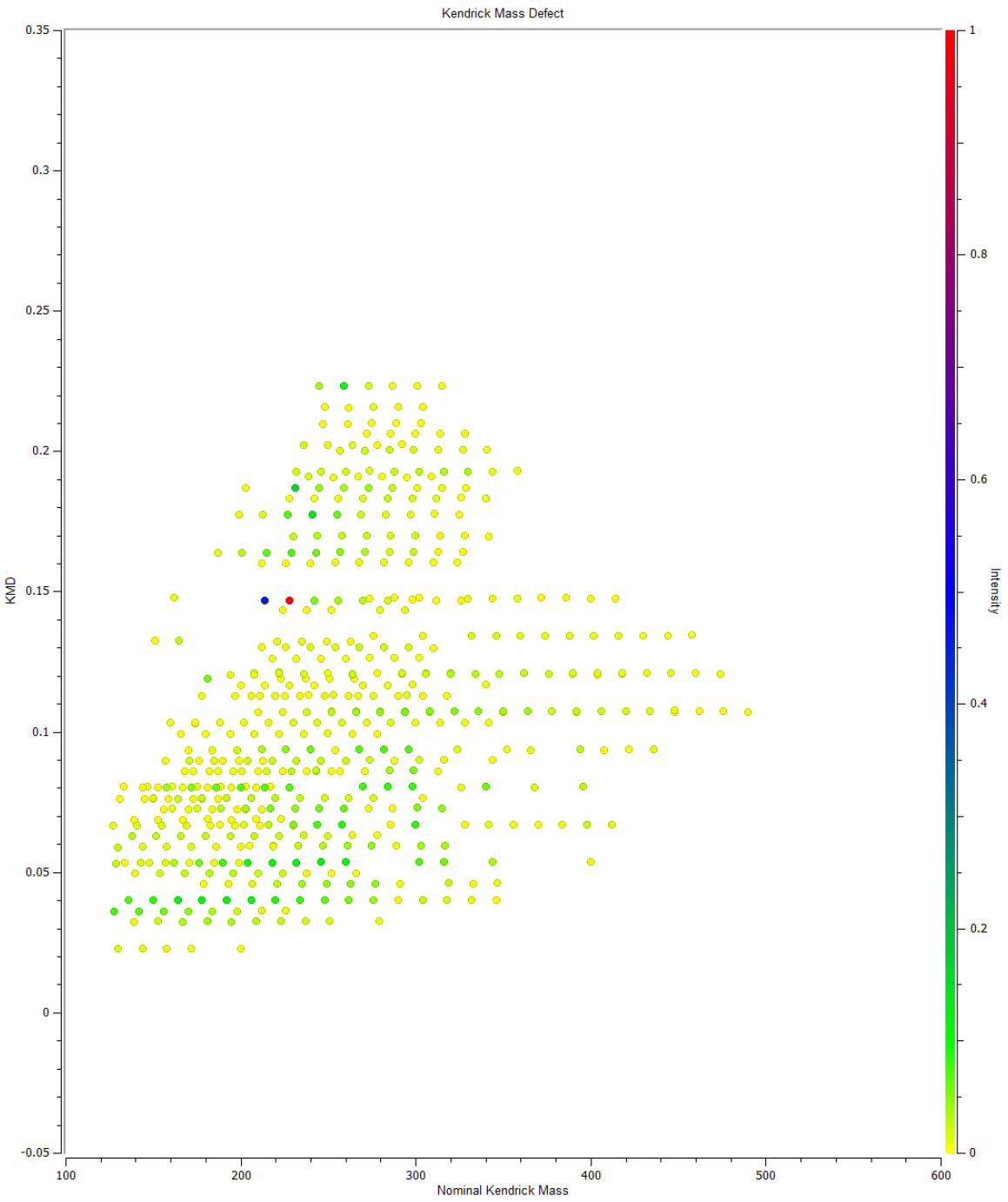

Figure 33: KMD Plot for SCO 06043. Aqueous alteration value of 1.2 with 525 molecular formulas identified.

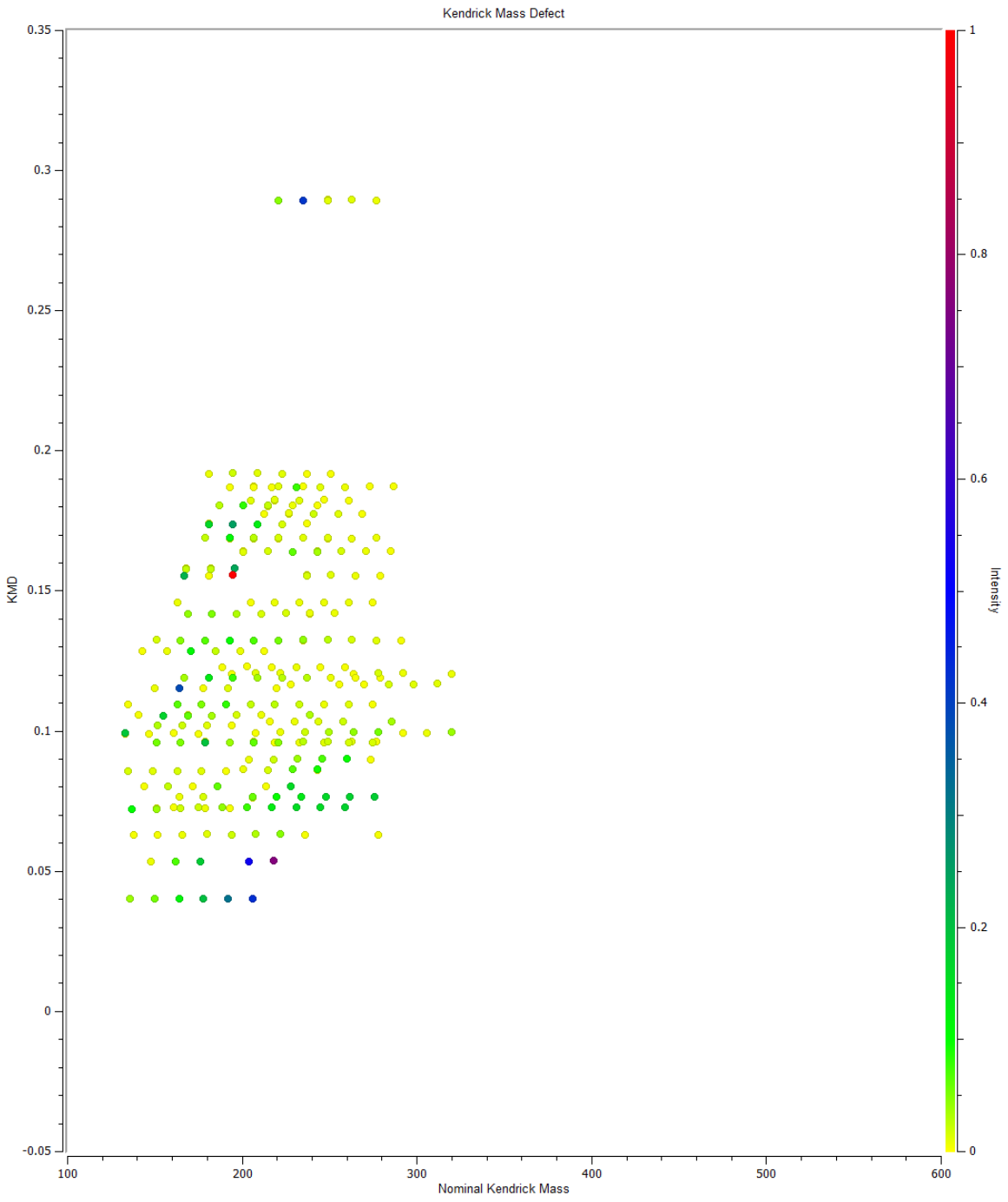

Figure 34: KMD Plot for ALH 83100. Aqueous alteration value of 1.1 with 246 molecular formulas identified.

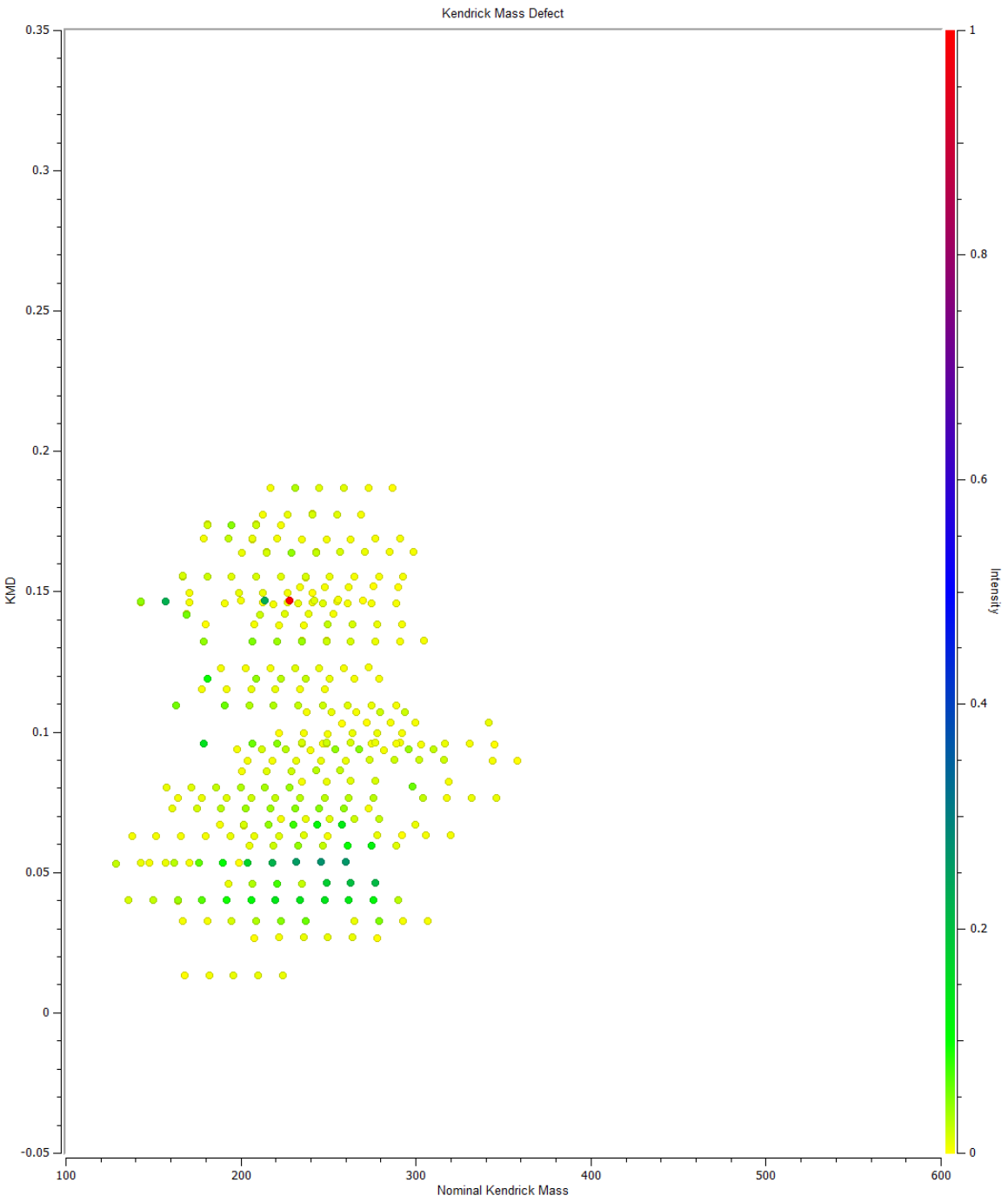

Figure 35: KMD Plot for ALH 84034. Aqueous alteration value of 1.1 with 299 molecular formulas identified.

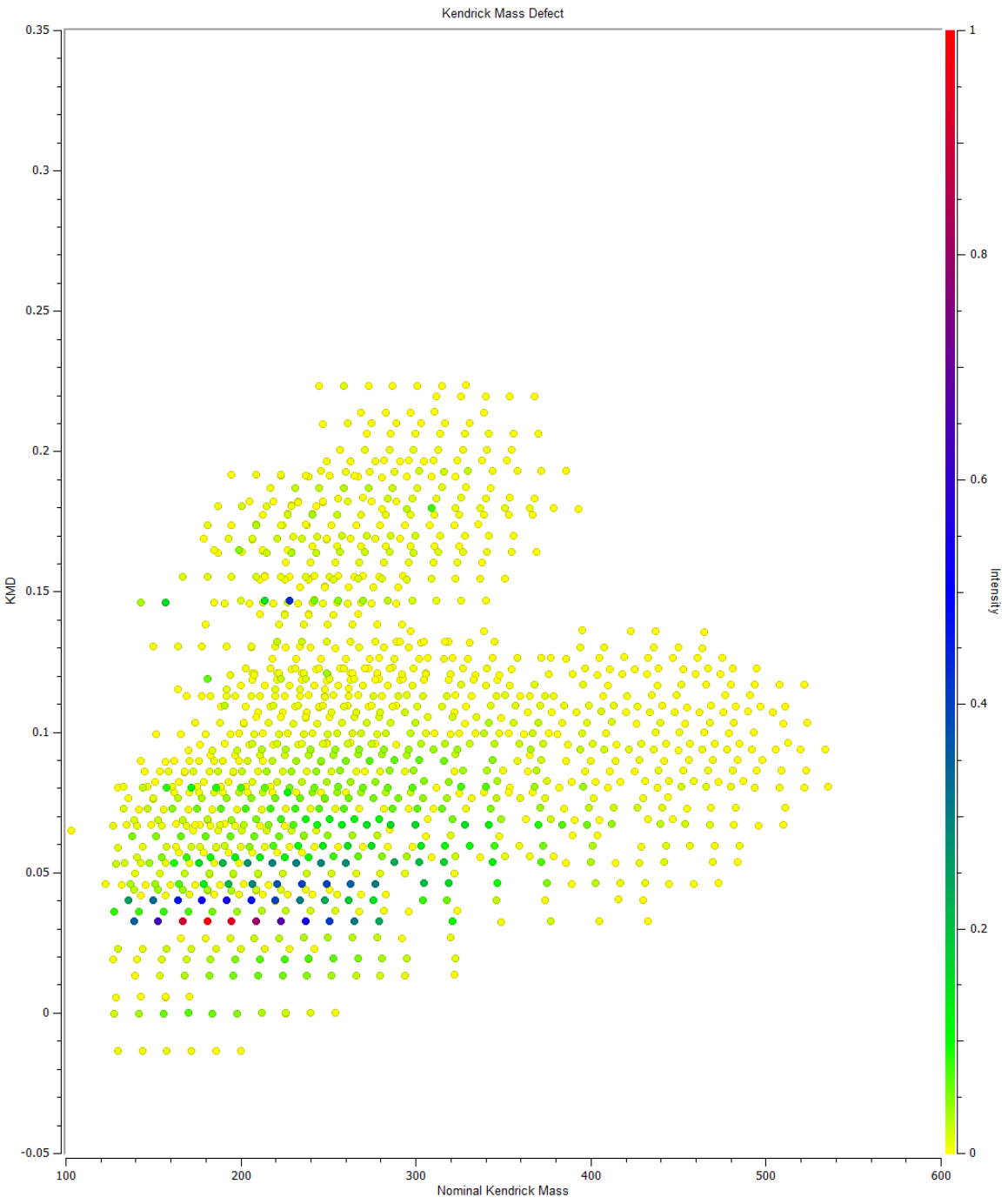

Figure 36: KMD Plot for DOM 08003. Aqueous alteration value of 1.1 with 1193 molecular formulas identified.

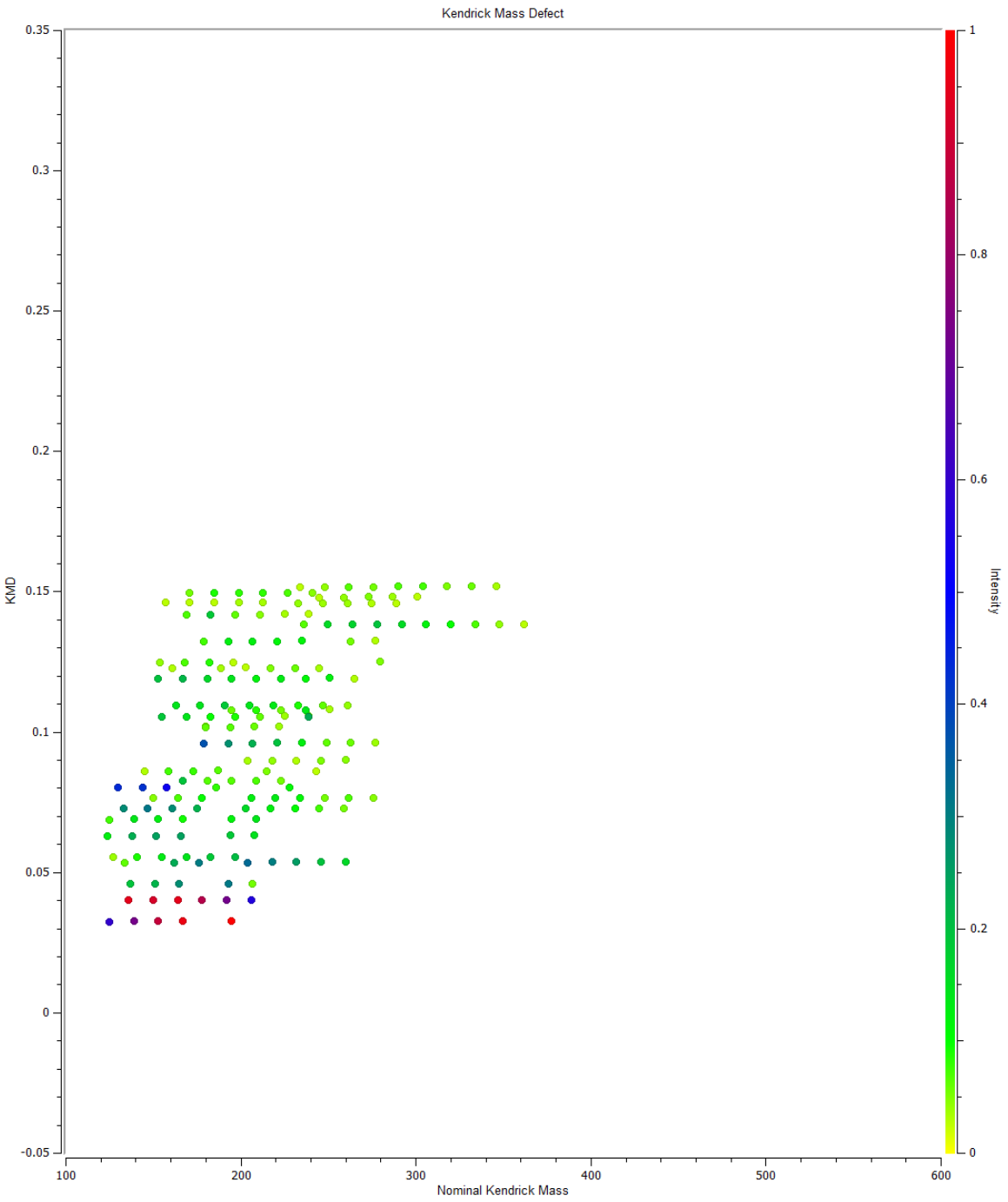

Figure 37: KMD Plot for LEW 85332. Aqueous alteration value has not been reported with 186 molecular formulas identified.

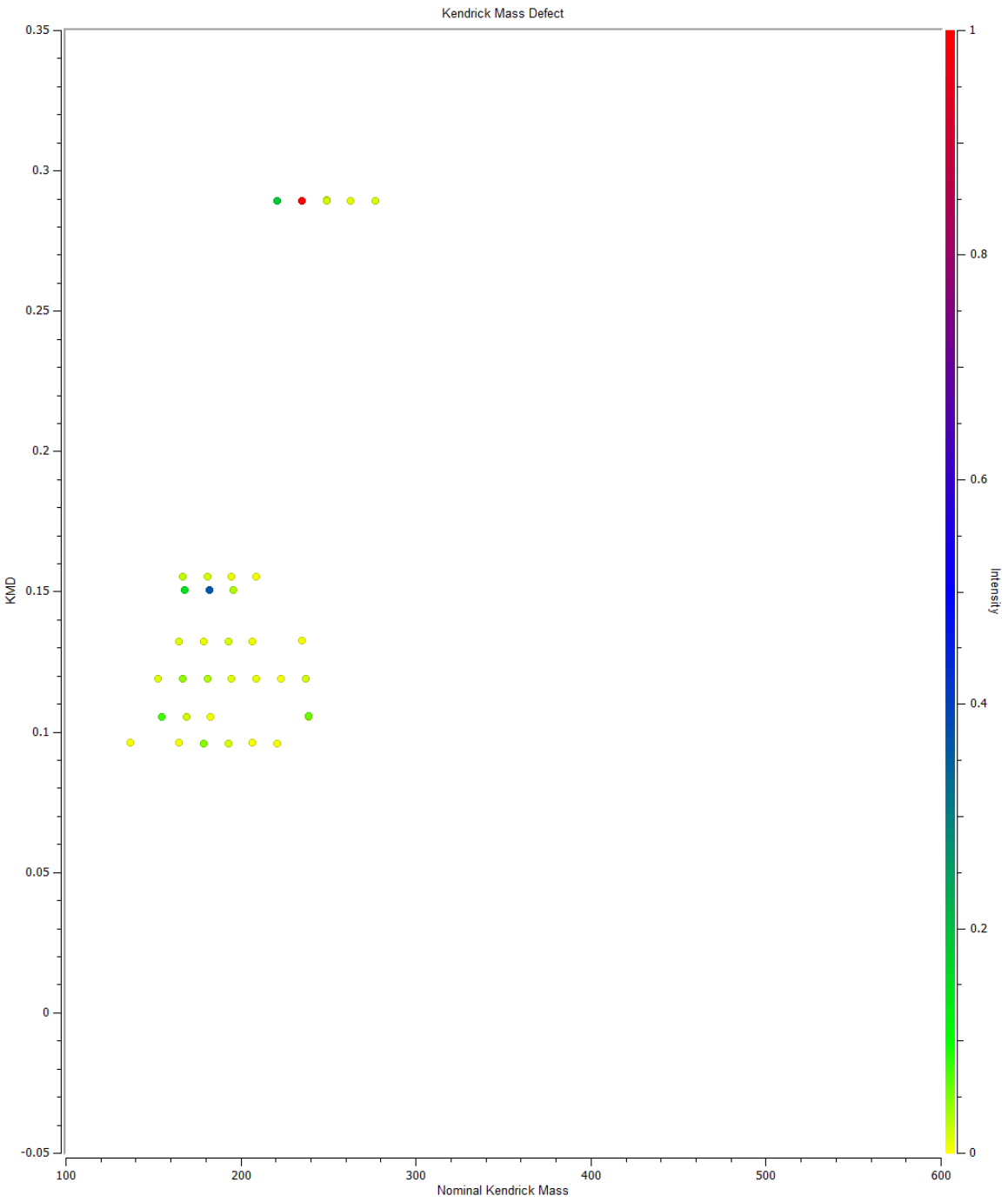

Figure 38: KMD Plot for MAC 87300. Aqueous alteration value has not been reported with 34 molecular formulas identified.

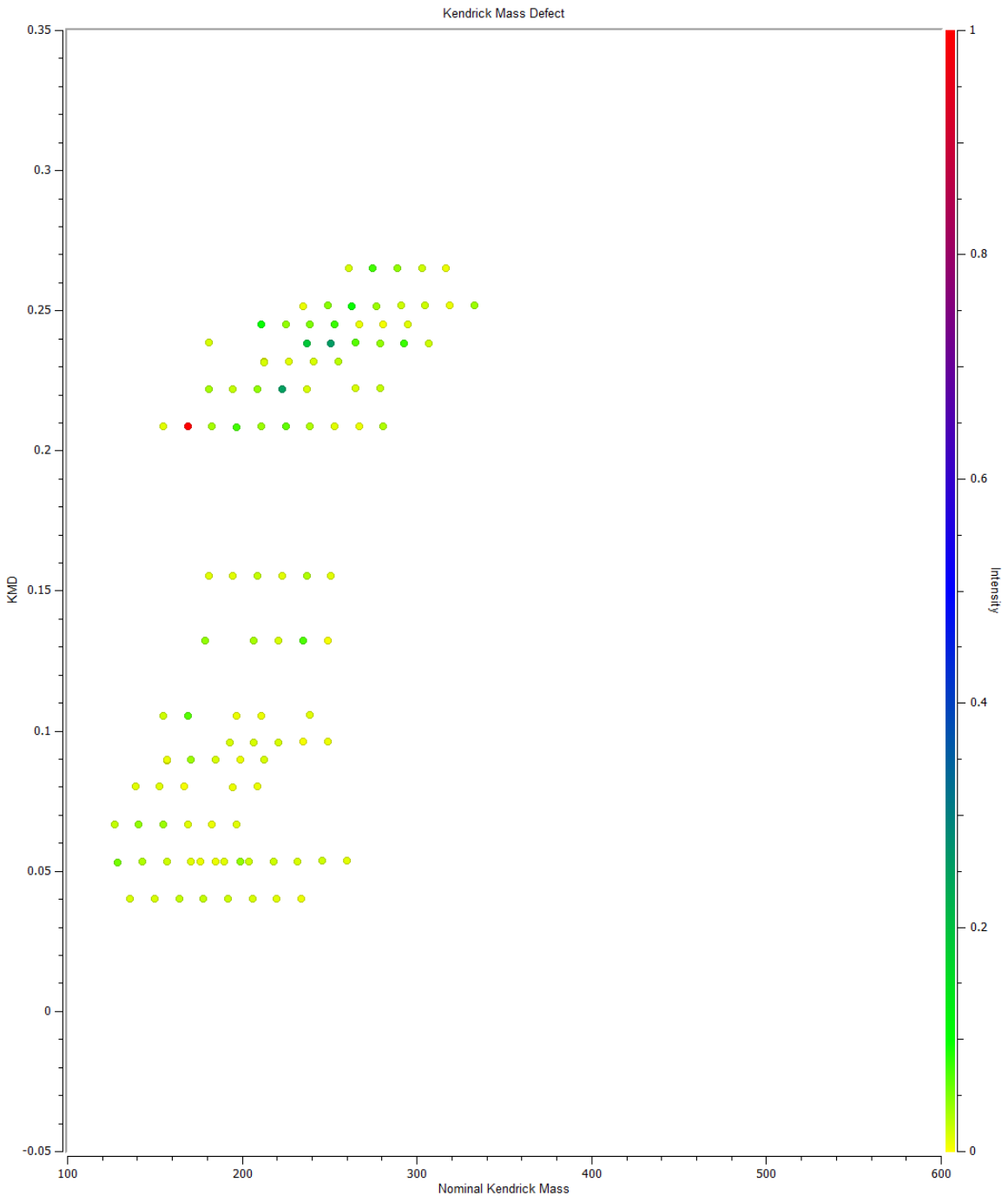

Figure 39: KMD Plot for MAC 88107. Aqueous alteration value has not been reported with 107 molecular formulas identified.

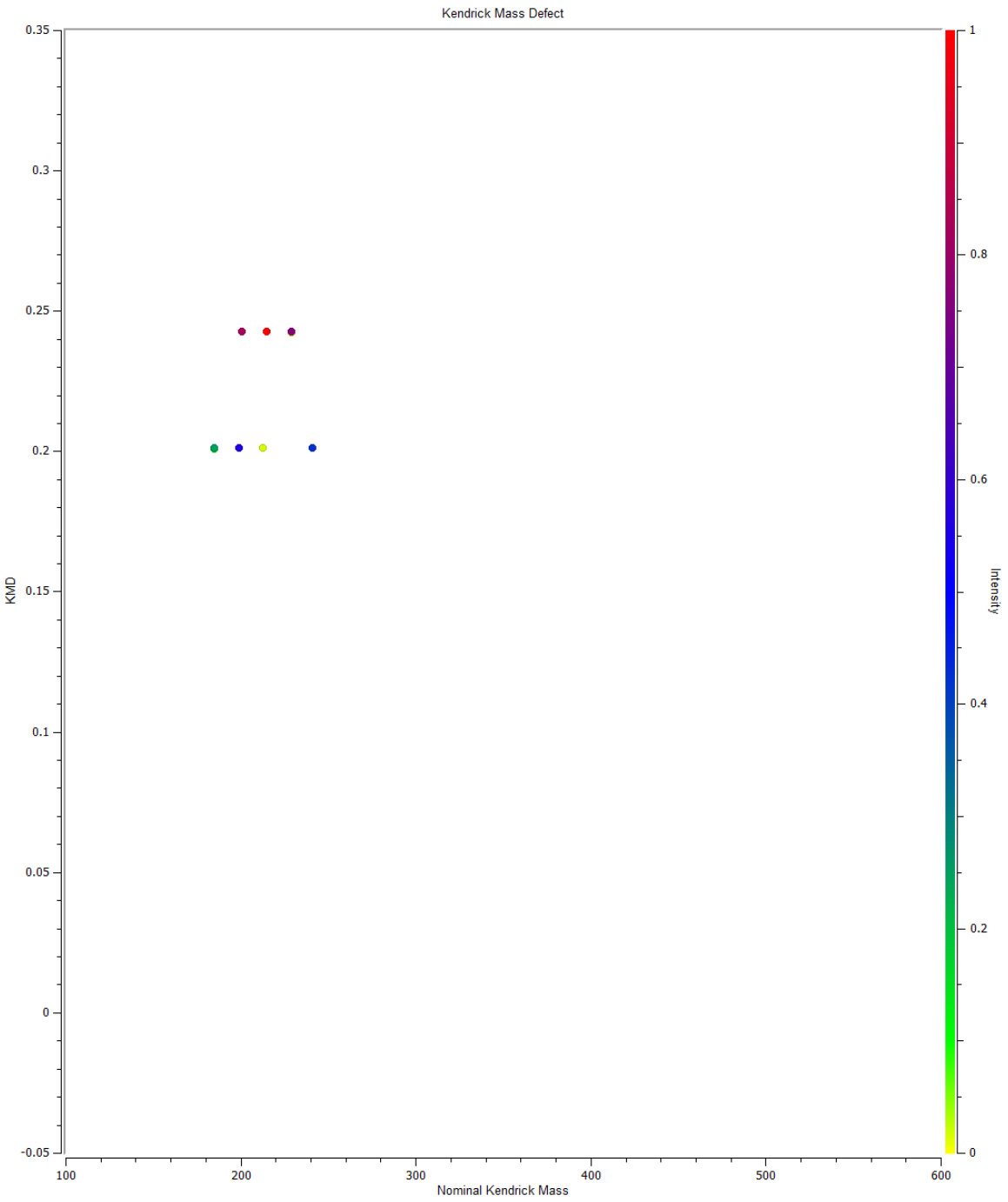

Figure 40: KMD Plot for PCA 02012. Aqueous alteration value has not been reported with 7 molecular formulas identified.

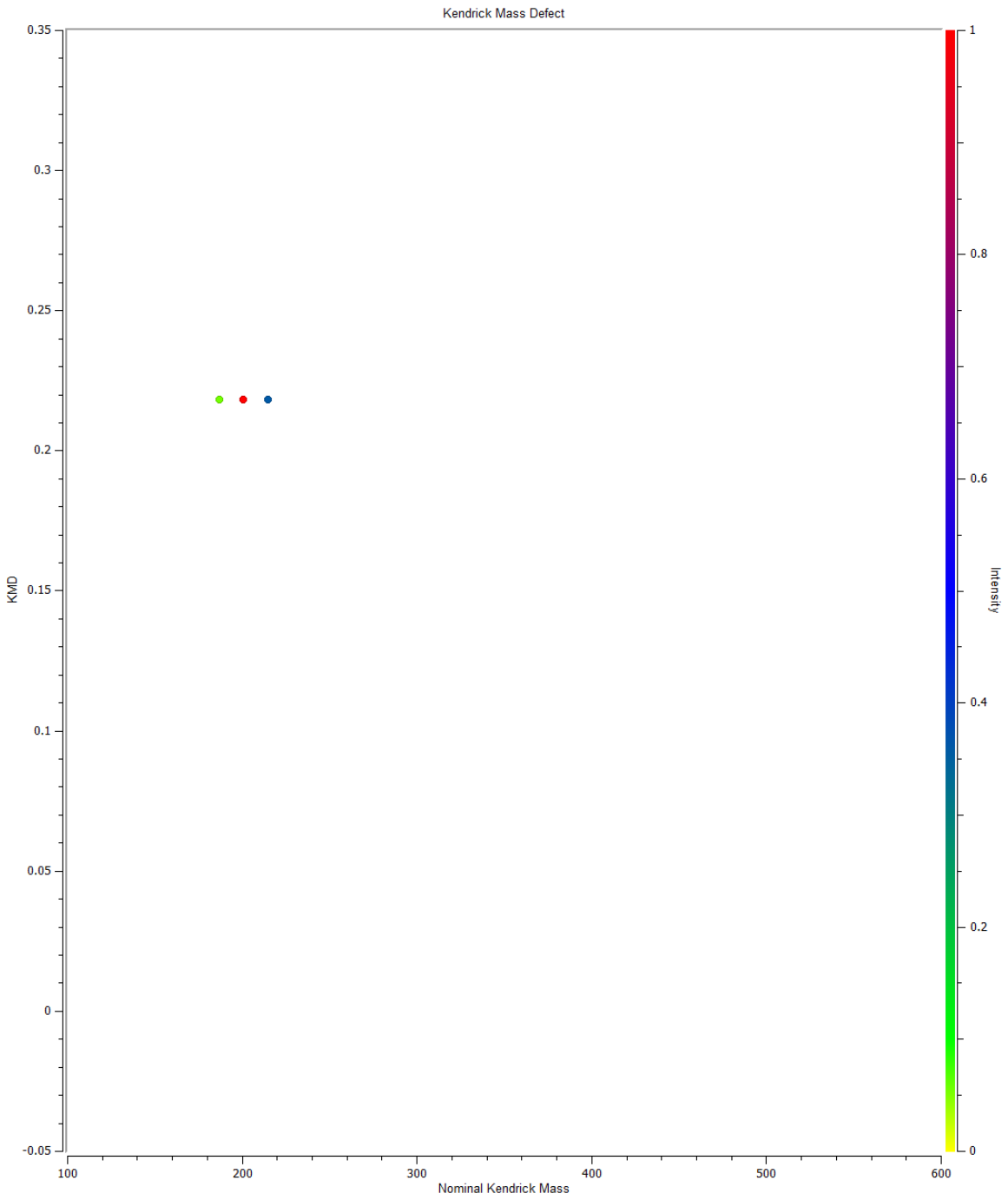

Figure 41: KMD Plot for QUE 99038. Aqueous alteration value has not been reported with 3 molecular formulas identified.

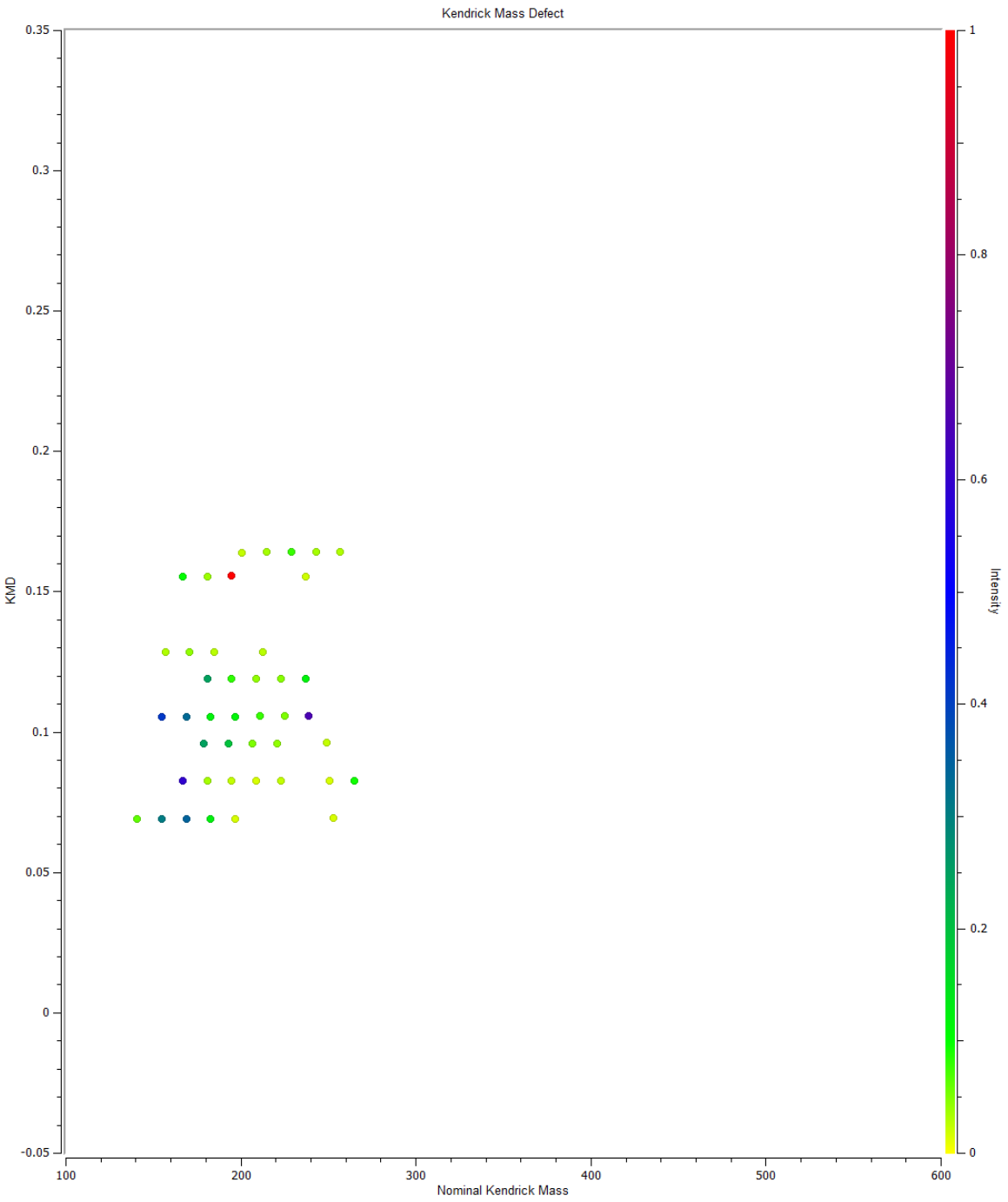

Figure 42: KMD Plot for WIS 91600. Aqueous alteration value has not been reported with 43 molecular formulas identified.